(12)



# FRACTURE MECHANICS OF DISSIMILAR MATERIALS BONDED THROUGH AN ORTHOTROPIC INTERFACIAL ZONE



by

Fazil Erdogan and Binghua Wu



Lehigh University, Bethlehem, PA

August 1992

FINAL PROJECT REPORT

OFFICE OF NAVAL RESEARCH CONTRACT NO. N0O014-89-3188

# FRACTURE MECHANICS OF DISSIMILAR MATERIALS BONDED THROUGH AN ORTHOTROPIC INTERFACIAL ZONE

by

Fazil Erdogan and Binghua Wu

Lehigh University, Bethlehem, PA

August 1992

FINAL PROJECT REPORT

OFFICE OF NAVAL RESEARCH CONTRACT NO. N0O014-89-3188



St-A per telecom, Mr. Rajatakse,
ONR/Code 1132sm, Arl., VA.
JK 10-16-92

# FRACTURE MECHANICS OF DISSIMILAR MATERIALS BONDED THROUGH AN ORTHOTROPIC INTERFACIAL ZONE

Fazil Erdogan* and Binghua Wu

Lehigh University, Bethlehem, PA 18015

Key words: Bonded Orthotropic Materials, Interface Cracks

## ABSTRACT

In this paper the fracture mechanics of orthotropic materials containing collinear interface cracks is considered. The primary objective is to study the influence of the thickness and the structure of the interfacial regions on the crack driving force. The interfacial region is assumed to be a relatively thin orthotropic elastic layer. The stress intensity factors or the strain energy release rates are assumed to be the main measure of the crack driving force. A relatively simple and efficient method is presented to solve the related elasticity problem. The results are obtained for a wide range of actual material combinations. In order to study the influence of the structure of the interfacial zone, the problem is also solved for isotropic and orthotropic materials bonded through a layer with hypothetically selected material properties. The results show that the effect

---

* Corresponding Author: Department of Mechanical Engineering and Mechanics, Lehigh University, Bethlehem, PA 18015; Tel. 215-758-4099, Fax. 215-758-5623

of the thickness, the mechanical properties and the material orientation of the interfacial zone on the strain energy release rate could be very significant. An interesting and a rather useful result obtained from the collinear crack solutions is that the strain energy release rates for multiple cracks in bonded orthotropic materials with or without an interfacial layer may predicted by using the results obtained for an isotropic homogeneous plane provided the normalization factors are selected properly.

## 1. Introduction

In recent past concerns with the mechanical failures initiating largely at the interfacial regions in such multiphase materials as modern composites, thermal barrier coatings and a variety of other bonded materials have led to rather extensive studies for the purpose of understanding the interaction between the flaws that may exist in these regions and the applied loads and other environmental factors [1], [2] and [3]. From the viewpoint of applications generally the optimal design of interfacial regions involves tradeoffs between strength and toughness. For example, it is known that the untreated carbon has very poor adhesion to epoxy and good adhesion can be accomplished by treating its surface and by using proper coupling agents (e.g., variety of silanes) [4]. However, joints of such high interfacial strength have usually rather poor toughness. Also considerations regarding load transfer and fiber integrity require a relatively weak or compliant interface. Thus, in studying the failure process of the interfacial regions the mechanical and strength parameters are expected to play a major role. In particular, in fracture related failures the crack driving force would heavily depend on the constitutive properties and the thickness of the interfacial zone, the size, location and the orientation of the crack and on the properties of the adherents as well as on the magnitude and the nature of the applied loads and the geometry of the medium [1]-[3], [5]-[8]. Since it is not likely to develop a process that would produce an interfacial zone

which would have all such desirable properties as high strength, high toughness, high fatigue and impact resistance and high resistance to moisture penetration, and since all these properties are quantitatively expressed in terms of continuum concepts, the fundamental studies relating to the chemistry of adhesion and material processing must, therefore, be guided by the corresponding mechanics considerations. It is through studying the appropriate mechanics particularly the fracture mechanics of the interfacial zones that the relative importance of certain material properties and dimensional parameters can be determined.

In most studies relating to the fracture mechanics of bonded materials it is generally assumed that the composite medium is piecewise homogeneous. On the other hand a close examination of these materials seems to indicate that in nearly all cases the interfacial region has a structure which is different than that of the adherents. In some cases this region may simply consist of the reaction zone and may have a thickness of only a few lattice parameters. In other bonded materials the interfacial regions having their own structure and thickness may develop as a result of surface preparations and coupling agents used in processing. For example, in many of the polymer matrix composites very near the interface crystallization of the polymer or copolymerization of the matrix and the coupling agent seems to produce a highly oriented region with a columnar or lamellar structure which may generally be modeled as a thin orthotropic layer (e.g., PEEK-Carbon composites) [4], [9]. Among other examples for such interfacial regions in bonded materials one may mention the grain boundaries and, at a larger length scale, certain geological materials such as shale - sandstone interfaces.

The main objective of this paper is to study the influence of the structure and the thickness of the interfacial regions on the fracture behavior of bonded orthotropic

materials. Specifically, the effect of two factors, namely, the material orthotropy and the multiple site cracking on the strain energy release rate will be investigated. Thus, the technique developed is suitable to study the general problem of collinear interfacial cracks in bonded orthotropic layers. In this paper, however, it will be assumed that the thickness of the adherents in comparison with the crack sizes and the interfacial zone thickness are sufficiently large so that the perturbation problem considered may be approximated by two dissimilar orthotropic half spaces bonded through an orthotropic layer. The interface crack problem for bonded semi-infinite orthotropic planes was previously considered in, for example, [10]-[12]. Among some of the significant recent studies dealing with the interface crack problems in bonded anisotropic half planes one may mention [13]-[15]. The problem of cracks perpendicular to and intersecting the interfaces in bonded orthotropic layers may be found in [16].

## 2. On the Formulation of the Problem

The plane strain collinear interface crack problem for two orthotropic half planes 1 and 3 bonded through an orthotropic interfacial layer 2 of thickness h is described in Fig. 1. To simplify the formulation of the problem the engineering elastic constants $E_{ij}$, $\nu_{ij}$ and $G_{ij}$, (i, j = 1, 2) for an orthotropic plane will be replaced by the "averaged" elastic parameters defined by [17], [18]

$$E_0 = \sqrt{E_{11}E_{22}}\ , \qquad \nu_0 = \sqrt{\nu_{12}\nu_{21}}\ ,$$

$$c^4 = E_{11}/E_{22}\ , \qquad \kappa_0 = \frac{E_0}{2G_{12}} - \nu_0 \tag{1}$$

for generalized plane stress, and

$$E_0 = \left[\frac{E_{11}E_{22}}{(1-\nu_{13}\nu_{31})(1-\nu_{23}\nu_{32})}\right]^{1/2}, \quad \nu_0 = \left[\frac{(\nu_{12}+\nu_{13}\nu_{32})(\nu_{21}+\nu_{23}\nu_{31})}{(1-\nu_{13}\nu_{31})(1-\nu_{23}\nu_{32})}\right]^{1/2},$$

$$c^4 = \frac{E_{11}}{E_{22}}\,\frac{(1-\nu_{23}\nu_{32})}{(1-\nu_{13}\nu_{31})}, \quad \kappa_0 = \frac{E_0}{2}\left(\frac{1}{G_{12}} - \frac{\nu_{21}+\nu_{23}\nu_{31}}{E_{22}} - \frac{\nu_{12}+\nu_{13}\nu_{32}}{E_{11}}\right). \tag{2}$$

for the case of plane strain. Thus, by using the contraction

$$y_1 = x_1/\sqrt{c}, \quad y_2 = x_2\sqrt{c}\ . \tag{3}$$

and defining

$$\tau_{11}(y_1,\ y_2) = \frac{1}{c}\ \sigma_{11}(x_1,\ x_2),\quad \tau_{12}(y_1,\ y_2) = \sigma_{12}(x_1,\ x_2),\quad \tau_{22}(y_1,\ y_2)=c\sigma_{22}(x_1,\ x_2), \tag{4}$$

$$v_1(y_1,\ y_2) = \sqrt{c}\ u_1(x_1,\ x_2),\quad v_2(y_1,\ y_2) = \frac{1}{\sqrt{c}}\ u_2(x_1,\ x_2), \tag{5}$$

the stress displacement relations may be expressed as

$$\frac{1}{c}\sigma_{11} = \tau_{11} = \frac{E_0}{1-\nu_0^{\,2}}\ (\frac{\partial v_1}{\partial y_1} + \nu_0\ \frac{\partial v_2}{\partial y_2}),$$

$$c\sigma_{22} = \tau_{22} = \frac{E_0}{1-\nu_0^{\,2}}\ (\frac{\partial v_2}{\partial y_2} + \nu_0\ \frac{\partial v_1}{\partial y_1}),$$

$$\sigma_{12} = \tau_{12} = \frac{E_0}{2(\kappa_0+\nu_0)}\ (\frac{\partial v_1}{\partial y_2} + \frac{\partial v_2}{\partial y_1}). \tag{6}$$

Here $x_i$, $\sigma_{ij}$ , and $u_i$, (i, j = 1, 2), are, respectively the physical coordinates, stresses and displacements. By substituting from (6) into the equilibrium conditions

$$\frac{\partial \sigma_{11}}{\partial x_1} + \frac{\partial \sigma_{12}}{\partial x_2} = 0, \quad \frac{\partial \sigma_{21}}{\partial x_1} + \frac{\partial \sigma_{22}}{\partial x_2} = 0, \tag{7}$$

it may be shown that

$$\beta_1\frac{\partial^2 v_1}{\partial y_1^{\,2}} + \frac{\partial^2 v_1}{\partial y_2^{\,2}} + \beta_2\frac{\partial^2 v_2}{\partial y_1 \partial y_2} = 0,$$

$$\frac{\partial^2 v_2}{\partial y_1^2} + \beta_1 \frac{\partial^2 v_2}{\partial y_2^2} + \beta_2 \frac{\partial^2 v_1}{\partial y_1 \partial y_2} = 0. \tag{8}$$

where

$$\beta_1 = \frac{2(\kappa_0 + \nu_0)}{1 - \nu_0^2} \ , \ \beta_2 = \frac{2\nu_0(\kappa_0 + \nu_0)}{1 - \nu_0^2} + 1 \ . \tag{9}$$

By using the standard Fourier Transforms the solution of (8) may be obtained as follows:

$$v_1(y_1, y_2) = \frac{1}{2\pi} \int_{-\infty}^{\infty} [C_1 e^{-s_1 |\alpha| y_2} + C_2 e^{-s_2 |\alpha| y_2} + C_3 e^{s_1 |\alpha| y_2} + C_4 e^{s_2 |\alpha| y_2}] \, e^{i\alpha y_1} \, d\alpha,$$

$$v_2(y_1, y_2) = \frac{1}{2\pi} \int_{-\infty}^{\infty} \frac{|\alpha| i}{\alpha} [\beta_3 C_1 e^{-s_1 |\alpha| y_2} + \beta_4 C_2 e^{-s_2 |\alpha| y_2} - \beta_3 C_3 e^{s_1 |\alpha| y_2} - \beta_4 C_4 e^{s_2 |\alpha| y_2}] \, e^{i\alpha y_1} \, d\alpha,$$

$$-\infty < y_1 < \infty \ , \ 0 < y_2 < h \ , \tag{10}$$

where the functions $C_i(\alpha)$, (i=1,...,4) are unknown.

$$\beta_3 = \frac{s_1 \beta_2}{\beta_1 s_1^2 - 1} \ , \ \beta_4 = \frac{s_2 \beta_2}{\beta_1 s_2^2 - 1} \ , \tag{11}$$

and $s_1$ and $s_2$ are the roots of the characteristic equation

$$s^4 - 2\kappa_0 s^2 + 1 = 0. \tag{12}$$

Equation (12) has four roots $s_1, \ldots, s_4$ given by

$$s_1 = -s_3 = \sqrt{\kappa_0 + \sqrt{\kappa_0^2 - 1}} \quad , \quad \mathrm{Re}(s_1) > 0.$$

$$s_2 = -s_4 = \sqrt{\kappa_0 - \sqrt{\kappa_0^2 - 1}} \quad , \quad \mathrm{Re}(s_2) > 0. \tag{13}$$

Note that the roots $s_1,\ldots, s_4$ depend on $\kappa_0$ only and they are all real for $\kappa_0 > 1$ and complex for $-1<\kappa_0<1$. For $\kappa_0 \leq -1$ the roots are pure imaginary for which equations (10) imply that the boundary value problem has no feasible solution. This restriction on $\kappa_0$ may also be arrived at by requiring that the elasticity matrix $C_{ij}$ (in $\sigma_i = C_{ij}\epsilon_j$) be positive definite [19]. From (1) and (2) it may easily be shown that for isotropic materials $\kappa_0 = 1$ and equations (8) and (12) reduce to the known results. Formally, equations (10) give the solution for an orthotropic layer where the constants $C_1,\ldots C_4$ are determined from the stress and/or displacement boundary conditions prescribed at $x_2 =$ constant planes.

## 3. Integral Equations for Collinear Cracks

Consider now the plane strain or plane stress collinear crack problem for two orthotropic half spaces bonded through an orthotropic layer described in Fig. 1. It is assumed that the elasticity problem for the composite medium has been solved under given applied loads by ignoring the cracks and the stresses $\sigma_{22}^0(x_1, 0)$ and $\sigma_{12}^0(x_1, 0)$ along the interface $x_2 = 0$ have been calculated. Thus, by using a superposition the original crack problem can be reduced to a perturbation problem in which the crack surface tractions $-\sigma_{22}^0(x_1, 0)$ and $-\sigma_{12}^0(x_1, 0)$ are the only external loads. Note that this process is rather straightforward if the stress state at infinity is zero and the applied loads consist of body forces and moments having finite resultants and acting within a bounded region of the medium. Otherwise, the stresses acting on the medium at infinity must be such that the strains $\epsilon_{11}$ along the interfaces $x_2 = 0$ and $x_2 = -h$ in the three

materials remain compatible. For example, if the applied loads at infinity are uniform tension $\sigma_{22}^{\infty} = \sigma_0$ and uniform shear $\sigma_{12}^{\infty} = \tau_0$, to maintain compatibility in the strains $\varepsilon_{11}$ or prevent any mismatch in the displacement components $u_1$ on $x_2 = 0$ and $x_2 = -h$, it would be necessary to apply to materials 1 and 2 the following additional external loads:

$$\sigma_{11}^{(1)}(\infty, x_2) = \sigma_0 E_{11}^{(1)} \left( \frac{\nu_{12}^{(1)}}{E_{11}^{(1)}} - \frac{\nu_{12}^{(3)}}{E_{11}^{(3)}} \right), \quad 0 < x_2 < \infty,$$

$$\sigma_{11}^{(2)}(\infty, x_2) = \sigma_0 E_{11}^{(2)} \left( \frac{\nu_{12}^{(2)}}{E_{11}^{(2)}} - \frac{\nu_{12}^{(3)}}{E_{11}^{(3)}} \right), \quad -h < x_2 < 0, \tag{14}$$

where the superscripts (1), (2) and (3) refer to materials 1, 2 and 3, respectively (Fig. 1).

The formulation given in the previous section is valid for each of the three materials shown in Fig. 1. An index $k = 1, 2, 3$ will be added to each quantity to designate the materials 1, 2 and 3, respectively. That is, the quantities which appear in Section 2 will be replaced by $x_{kl}$, $y_{kl}$, $E_{k0}$, $\nu_{k0}$, $c_k$, $u_{kl}$, $v_{kl}$, $\sigma_{kil}$, $\tau_{kil}$, $s_{kl}$, $\beta_{kj}$, $C_{kj}$, ($k = 1, 2, 3$; $i = 1, 2$; $l = 1, 2$; $j = 1, 2, 3, 4$). Referring now to (10), since the displacements in the medium vanish at $x_2 = \mp\infty$ or $y_2 = \mp\infty$, we must have

$$C_{13} = 0, \quad C_{14} = 0, \quad C_{31} = 0, \quad C_{32} = 0. \tag{15}$$

The remaining eight functions are then determined by using the continuity and boundary conditions at $x_2 = 0$ and $x_2 = -h$. These conditions may be expressed as (Fig. 1)

$$\sigma_{122}(x_1, 0) = \sigma_{222}(x_1, 0), \quad \sigma_{112}(x_1, 0) = \sigma_{212}(x_1, 0), \quad -\infty < x_1 < \infty, \tag{16}$$

$$\sigma_{222}(x_1, -h) = \sigma_{322}(x_1, -h), \quad \sigma_{212}(x_1, -h) = \sigma_{312}(x_1, -h), \quad -\infty < x_1 < \infty. \tag{17}$$

$$u_{21}(x_1, -h) = u_{31}(x_1, -h), \quad u_{22}(x_1, -h) = u_{32}(x_1, -h), \quad -\infty < x_1 < \infty. \tag{18}$$

$$\sigma_{122}(x_1, 0) = -\sigma_{22}^{0}(x_1, 0) = p_1(x_1), \quad \sigma_{112}(x_1, 0) = -\sigma_{12}^{0}(x_1, 0) = p_2(x_1), \; x_1 \in L, \tag{19}$$

$$u_{11}(x_1, 0) - u_{21}(x_1, 0) = 0, \quad u_{12}(x_1, 0) - u_{22}(x_1, 0) = 0, \qquad x_1 \in L', \tag{20}$$

$$L = \sum_{j=1}^{n} L_j, \qquad L_j = (a_j < x_1 < b_j), \quad j = 1, \ldots, n, \tag{21}$$

where $p_1$ and $p_2$ are known functions, $L_j$ represents the jth crack (Fig. 1), and $L'$ is the complement of L in $(-\infty, \infty)$.

By using (15) and substituting from (10) into the homogeneous equations (16) – (18), six of the unknown functions $C_{kj}$ may be eliminated, the two remaining unknowns are then determined by using the mixed boundary conditions (19) and (20). To reduce (19) and (20) to a system of integral equations we define

$$\frac{\partial}{\partial x_1}\left[ u_{11}(x_1, 0) - u_{21}(x_1, 0)\right] = f_1(x_1), \qquad -\infty < x_1 < \infty,$$

$$\frac{\partial}{\partial x_1}\left[ u_{12}(x_1, 0) - u_{22}(x_1, 0)\right] = f_2(x_1), \qquad -\infty < x_1 < \infty. \tag{22}$$

From (20) and (22) it follows that

$$f_k(x_1) = 0, \quad (k = 1, 2), \qquad x_1 \in L'. \tag{23}$$

$$\int_{L_i} f_k(x_1)\, dx_1 = 0. \quad (k = 1, 2;\ i = 1, \ldots, n). \tag{24}$$

It is seen that by substituting from (10) into (16), (17), (18) and (22) all eight unknown functions $C_{kj}$ may be expressed in terms of $f_1$ and $f_2$. Equations (19) would then give a pair of integral equations to determine $f_1$ and $f_2$. This process is somewhat lengthy but straightforward. Thus, referring to [20] for analytical details we obtain

$$\gamma_{11} f_1(x_1) + \gamma_{12} \frac{1}{\pi} \int_L \frac{f_2(t)}{t-x_1}\, dt + \frac{1}{\pi} \int_L \sum_{j=1}^{2} K_{1j}(x_1, t) f_j(t) dt = p_1(x_1), \quad x_1 \in L,$$

$$\gamma_{21} \frac{1}{\pi} \int_L \frac{f_1(t)}{t-x_1}\, dt + \gamma_{22} f_2(x_1) + \frac{1}{\pi} \int_L \sum_{j=1}^{2} K_{2j}(x_1, t) f_j(t) dt = p_2(x_1), \quad x_1 \in L. \tag{25}$$

where $K_{ij}$, (i, j = 1, 2) are known bounded functions and the bimaterial constants $\gamma_{ij}$, (i, j = 1, 2) are given by (see [20])

$$\gamma_{ij} = \frac{n_{ij}}{n_0}, \qquad (i, j = 1, 2), \tag{26}$$

$$n_{11} = -n_{22} = \frac{1-\nu_{20}}{E_{20}} - \frac{1-\nu_{10}}{E_{10}}, \quad n_{12} = \frac{\sqrt{2(1+\kappa_{10})}}{c_1 E_{10}} + \frac{\sqrt{2(1+\kappa_{20})}}{c_2 E_{20}},$$

$$n_{21} = \frac{c_1\sqrt{2(1+\kappa_{10})}}{E_{10}} + \frac{c_2\sqrt{2(1+\kappa_{20})}}{E_{20}}, \quad n_0 = n_{12} n_{21} - n_{11}^2. \tag{27}$$

The elastic constants which appear in (27) are defined by (1) or (2). Note that $\gamma_{12}$ and $\gamma_{21}$ are always positive.

The integral equations (25) may further be simplified by defining

$$\gamma = \frac{\beta_{11}}{\sqrt{\beta_{12}\beta_{21}}}, \quad \eta = \sqrt{\frac{\beta_{21}}{\beta_{12}}}, \tag{28}$$

$$f(x_1) = \eta^{-1} f_2(x_1) + i\, f_1(x_1), \quad p(x_1) = p_2(x_1) + i\,\eta\, p_1(x_1), \quad x_1 \in L. \tag{29}$$

Thus by using (28) and (29) and combining (25) it may easily be shown that

$$\frac{1}{\pi i}\int_L \frac{f(t)}{t - x_1}\,dt + \gamma\, f(x_1) + \frac{1}{\pi}\int_L [K_1(x_1, t)\, f(t) + K_2(x_1, t)\,\overline{f}(t)]dt = \frac{1}{\beta_{21}}\, p(x_1), \qquad x_1 \in L, \tag{30}$$

where

$$K_1(x_1, t) = \frac{1}{2\sqrt{\beta_{12}\beta_{21}}}\left[K_{22} - K_{11} - i\left(\frac{1}{\eta}\, K_{21} + \eta K_{12}\right)\right],$$

$$K_2(x_1, t) = \frac{1}{2\sqrt{\beta_{12}\beta_{21}}}\left[K_{22} + K_{11} + i\left(\frac{1}{\eta}\, K_{21} - \eta K_{12}\right)\right]. \tag{31}$$

For the case of n collinear cracks $L_1, \ldots, L_n$, theoretically the index of the singular integral equation (30) is n and, consequently, its solution contains n arbitrary (complex) constants. These constants may be obtained from the single-valuedness conditions (24) which may now be expressed as

$$\int_{a_j}^{b_j} f(t)\,dt = 0, \qquad j = 1, \ldots, n. \tag{32}$$

## 4. The Method of Solution

Trying to solve the integral equation (30) which is defined on the union of n arcs $L_1, \ldots, L_n$ directly is highly impractical. It is, however, rather easy to reduce (30) to a

system of n simpler integral equations each of which is defined on a single arc $L_j$. Thus, by defining

$$t = \frac{b_j - a_j}{2} s + \frac{b_j + a_j}{2}, \quad a_j < t < b_j, \quad -1 < s < 1,$$

$$x_1 = \frac{b_k - a_k}{2} r + \frac{b_k + a_k}{2}, \quad a_k < x_1 < b_k, \quad -1 < r < 1, \tag{33}$$

$$f(t) = v_j(s), \ a_j < t < b_j; \quad p(x_1) = q_k(r), \ a_k < x_1 < b_k, \tag{34}$$

$$K_1(x_1, t) = R_{kj}(r, s), \quad K_2(x_1, t) = S_{kj}(r, s), \quad a_k < x_1 < b_k, \ a_j < t < b_j, \tag{35}$$

$$h_{kj}(r, s) = \frac{b_j - a_j}{(b_j - a_j)\, s - (b_k - a_k)\, r + b_j + a_j - b_k - a_k} = \frac{1}{s - z_{kj}}, \tag{36}$$

from (30) it may easily be seen that

$$\frac{1}{\pi i} \int_{-1}^{1} \frac{v_k(s)}{s - r}\, ds - \gamma_{21} v_k(r) + \frac{1}{\pi i} \sum_{j=1}^{n}{}' \int_{-1}^{1} h_{kj}(r, s) v_j(s) ds$$

$$+ \sum_{j=1}^{n} \frac{b_j - a_j}{2} \int_{-1}^{1} [R_{kj}(r, s) v_j(s) + S_{kj}(r, s) \bar{v}_j(s)] ds = \frac{1}{\gamma_{21}} q_k(s),$$

$$k = 1, \ldots, n, \quad -1 < r < 1, \tag{37}$$

where the prime in the third term indicates that the summation excludes the term corresponding to $j = k$. Note that the kernels $h_{kj}(r, s)$ as well as $R_{kj}$ and $S_{kj}$ are bounded in the closed interval $-1 \le (r, s) \le 1$. The unknown functions $v_k$ and known functions $q_k$ respectively represent the crack opening displacements and the crack

surface tractions for the kth crack $L_k$.

We now observe that the weight function of $\psi_k(s)$ in (37) is [20], [21]

$$w(r) = (1-r)^{\alpha}(1+r)^{\beta}, \quad -1 < r < 1, \tag{38}$$

where

$$\alpha = -\frac{1}{2} - i\omega, \qquad \beta = -\frac{1}{2} + i\omega, \qquad \omega = \frac{1}{2\pi}\log\left(\frac{1+\gamma}{1-\gamma}\right). \tag{39}$$

The orthogonal polynomials associated with w(r) are the Jacobi polynomials $P_n^{(\alpha,\beta)}(r)$ and therefore the solution of (37) may be expressed as

$$\psi_k(r) = g_k(r)w(r), \quad g_k(r) = \sum_{j=0}^{\infty} A_{kj} P_j^{(\alpha,\beta)}(r), \quad -1 < r < 1, \ k = 1,\ldots,n, \tag{40}$$

where $A_{kj}$ are unknown complex constants. From (34) it may be seen that the conditions (32) become

$$\int_{-1}^{1} \psi_k(r)dr = 0, \quad k = 1,\ldots, n. \tag{41}$$

Thus, by using the orthogonality conditions for the Jacobi polynomials, from (40) and (41) we find

$$A_{k0} = 0, \ k = 1,\ldots, n. \tag{42}$$

The singular integral equations (37) may be regularized by using the following property of the Jacobi polynomials:

$$\frac{1}{\pi i}\int_{-1}^{1} w(s)P_n^{(\alpha,\beta)}(s)\frac{ds}{s-r} - \gamma\, w(r)P_n^{(\alpha,\beta)}(r) = \frac{\sqrt{1-\gamma^2}}{2i}P_{n-1}^{(-\alpha,-\beta)}(r), \quad -1 < r < 1. \tag{43}$$

Thus, by substituting from (43) into (37) the singular terms in the integral equations may be removed and (37) may be reduced to a system of functional equations with $A_{kj}$, (k = 1.... n; j = 1, 2, 3...) as the unknown coefficients. These equations may be solved by truncating the series defined in (40) at $j = N_k$ and by using a method of collocation. For improved accuracy in each equation the collocation points $r_m$ are selected as

$$T_{N_k}(r_m) = 0 \ , \ \ r_m = \cos\theta_m \ , \ \ \theta_m = \frac{\pi}{2N_k}(2m-1) \ , \ \ m = 1....N_k, \ k = 1.... \ n. \qquad (44)$$

The integral equations (37) may then be reduced to a system $N_1 + .. + N_n$ linear algebraic equations in $A_{kj}$, (k = 1.... n, j = 1.... $N_k$). It should be noted that in addition to the first two terms, the third term involving the kernels $h_{kj}$ in (37) can also be evaluated in closed form [20]. Furthermore, the integrals in the fourth term are all Gaussian type and may be calculated rather accurately without any difficulty.

## 5. Stress Intensity Factors and the Strain Energy Release Rate

It may be seen that once the coefficients $A_{kj}$ are determined, (40) essentially provides a closed form solution. From a view point of fracture mechanics generally the quantities of interest are the crack opening displacement, the stress intensity factors and the strain energy release rate. From (22), (29), (33) and (34) the crack opening displacement may be expressed as

$$v_k(x_1) = \frac{1}{\eta}\,(u_{12}^{+} - u_{22}^{-}) + i(u_{11}^{+} - u_{21}^{-}) = \int_{a_k}^{x_1} f(t)dt$$

$$= \frac{b_k - a_k}{2} \int_{-1}^{r} v_k(s)ds. \qquad k = 1.... \ n. \qquad (45)$$

Substituting now from (40) and evaluating the integral [20] we find

$$v_k(x_1) = -\frac{b_k - a_k}{2} \sum_{j=1}^{\infty} \frac{1}{2_j} A_{kj} \sqrt{1-r^2}\, \left(\frac{1+r}{1-r}\right)^{i\omega} P_{j-1}^{(\alpha+1,\beta+1)}(r) \,, \qquad -1 < r < 1,$$

$$r = \frac{2}{b_k - a_k}\left(x_1 - \frac{b_k + a_k}{2}\right) \,, \quad k=1,\ldots, n. \tag{46}$$

In the mixed boundary value problems such as that under consideration it may be shown that the fundamental solution or the weight function w(r) defined by (38) represents the asymptotic behavior of stresses and displacements near the crack tips. In this problem w(r) has complex singularities. Thus, one may define a complex stress intensity factor as follows:

$$k(b_k) = \eta k_1 + i k_2 = \lim_{x_1 \to b_k} \sqrt{2}\, (x_1 - b_k)^{-\alpha} [\, \eta \sigma_{22}(x_1, 0) + i\sigma_{12}(x_1, 0)],$$

$$k(a_k) = \eta k_1 + i k_2 = \lim_{x_1 \to a_k} \sqrt{2}\, (a_k - x_1)^{-\beta} [\, \eta \sigma_{22}(x_1, 0) + i\sigma_{12}(x_1, 0)],$$

$$k = 1\ldots, n. \tag{47}$$

Observing that left hand side of (30) represents the stresses on L′ as well as on L, referring to [20] for details the stress intensity factors defined by (47) may expressed as follows:

$$k(b_k) = -\gamma_{21}\sqrt{1-\gamma^2}\, (b_k - a_k)^{i\omega} g_k(1)\sqrt{(b_k - a_k)/2} \,,$$

$$k(a_k) = \gamma_{21}\sqrt{1-\gamma^2}\, (b_k - a_k)^{-i\omega} g_k(-1)\sqrt{(b_k - a_k)/2} \,, \tag{48}$$

where $g_k(r)$ is given by (40). Similarly in [20] it was shown that from the "crack closure energy" the strain energy release rate may be evaluated as

$$\mathcal{G}(b_k) = \frac{\pi k(b_k)\bar{k}(b_k)}{4\gamma_{21}} \,, \quad \mathcal{G}(a_k) = \frac{\pi k(a_k)\bar{k}(a_k)}{4\gamma_{21}} \,. \tag{49}$$

where the elastic constant $\gamma_{21}$ is given by (26) and (27) and the bars refer to complex conjugates.

## 6. The Special Cases

In this section we give the results for some simple special cases for which the solution may be obtained in closed form.

(a) A single interface crack $(-a, a)$ in two bonded dissimilar half planes ($n = 1$, $h = \infty$, Fig.1)

In this case the Fredholm kernels $K_1$ and $K_2$ in (31) are zero and the solution may be expressed in closed form [20]. In particular for a uniform stress state $\sigma_0$, $\tau_0$ at infinity, or for

$$\sigma_{22}(x_1, 0) = -\sigma_0, \quad \sigma_{12}(x_1, 0) = -\tau_0, \tag{50}$$

we obtain

$$A_1 = -\frac{2}{\sqrt{1-\gamma^2}}\left(\frac{\sigma_0}{\sqrt{\gamma_{12}\gamma_{21}}} + i\frac{\tau_0}{\gamma_{21}}\right), \quad A_k = 0, \; k = 2, 3, \ldots. \tag{51}$$

giving

$$v(x_1) = \frac{2}{\sqrt{1-\gamma^2}}\left(\frac{\sigma_0}{\sqrt{\gamma_{12}\gamma_{21}}} + i\frac{\tau_0}{\gamma_{21}}\right)\sqrt{a^2 - x_1^2}\left(\frac{a+x_1}{a-x_1}\right)^{i\omega}, \tag{52}$$

$$k(a) = (2a)^{i\omega}(1-2i\omega)(\eta\sigma_0 + i\tau_0)\sqrt{a},$$

$$k(-a) = (2a)^{-i\omega}(1+2i\omega)(\eta\sigma_0 + i\tau_0)\sqrt{a}, \tag{53}$$

$$\mathcal{G} = \frac{\pi}{4}\frac{1+4\omega^2}{\gamma_{21}}(\eta^2\sigma_0^2 + \tau_0^2)a, \tag{54}$$

where the elastic constants are defined by (26)-(28) and (39), and 2a is the crack length.

(b) Homogeneous orthotropic medium with a single crack ( – a, a)

In this case we have

$$\gamma = 0, \quad \omega = 0, \quad \gamma_{12} = \frac{1}{2\sqrt{2}} \frac{E_0}{c\sqrt{1+\kappa_0}} \quad , \quad \gamma_{21} = \frac{1}{2\sqrt{2}} \frac{E_0 c}{\sqrt{1+\kappa_0}} \, . \tag{55}$$

the crack tip stress fields become uncoupled and from (49) mode I and mode II components of the strain energy release rate may be obtained as follows:

$$\mathcal{G}_1 = \frac{\pi k_1^{\,2}}{4\gamma_{12}} \, , \qquad \mathcal{G}_2 = \frac{\pi k_2^{\,2}}{4\gamma_{21}} \, . \tag{56}$$

If the applied loads are given by (50), we find

$$k_1 = \sigma_0\sqrt{a} \, , \qquad k_2 = \tau_0\sqrt{a} \, . \tag{57}$$

$$\mathcal{G}_1 = \frac{\pi\sigma_0^{\,2}a}{4\gamma_{12}} \, , \quad \mathcal{G}_2 = \frac{\pi\tau_0^{\,2}a}{4\gamma_{21}} . \tag{58}$$

If the medium is homogeneous and isotropic with the elastic constants $\mu$ and $\kappa$ we have

$$\gamma = 0, \quad \omega = 0, \quad \gamma_{12} = \gamma_{21} = \frac{2\mu}{1+\kappa} \, , \quad \mathcal{G}_j = \frac{1+\kappa}{8\mu}\pi k_j^{\,2} \, , \quad (j=1, 2), \tag{59}$$

where $\mu$ is the shear modulus and $\kappa = 3 - 4\nu$ for plane strain and $\kappa = (3-\nu)/(1+\nu)$ for plane stress conditions and for uniform loading $k_1$ and $k_2$ are given by (57).

(c) Bonded isotropic half planes with a single crack ( – a, a)

If the two half planes are isotropic having the elastic constants $\mu_1$, $\kappa_1$ and $\mu_2$, $\kappa_2$, we have

$$\gamma_{12} = \gamma_{21} = \frac{\mu_1\mu_2[\mu_1(\kappa_2+1)+\mu_2(\kappa_1+1)]}{(\mu_1+\mu_2\kappa_1)(\mu_2+\mu_1\kappa_2)} \, .$$

$$\gamma_{11} = -\frac{\mu_1\mu_2[\mu_2(\kappa_1-1)-\mu_1(\kappa_2-1)]}{(\mu_1+\mu_2\kappa_1)(\mu_2+\mu_1\kappa_2)} \quad .$$

$$\gamma = \frac{\gamma_{11}}{\sqrt{\gamma_{12}\gamma_{21}}} = \frac{\mu_1(\kappa_2-1)-\mu_2(\kappa_1-1)}{\mu_1(\kappa_2+1)+\mu_2(\kappa_1+1)} \quad . \tag{60}$$

and from (49) we obtain [6]

$$\mathcal{G} = \frac{\pi k\bar{k}}{4}(1-\gamma^2)\left(\frac{\kappa_2+1}{4\mu_2}+\frac{\kappa_1+1}{4\mu_1}\right) \quad . \tag{61}$$

In the case of uniform applied loads (50) the stress intensity factors are again given by (53) with $\eta = 1$.

(d) Homogeneous isotropic plane with two collinear cracks of equal length

To provide a benchmark for the collinear interface crack results we give the solution for an isotropic plane having two collinear cracks of equal length. Referring to Fig. 1, let $a_1 = -B$, $b_1 = -A$, $a_2 = A$ and $b_2 = B$. For uniform tension $\sigma_{22} = \sigma_0$ at $x_2 = \mp\infty$ the mode I stress intensity factors may be expressed as [22]

$$k_1(A) = \frac{\sigma_0\sqrt{A}}{\sqrt{(B^2/A^2)-1}}\left[(B^2/A^2)\,E(k)/K(k)-1\right] .$$

$$k_1(B) = \frac{\sigma_0\sqrt{B}}{\sqrt{1-(A^2/B^2)}}\left[1-E(k)/K(k)\right] . \quad k^2 = 1-(A^2/B^2) . \tag{62}$$

where $K(k)$ and $E(k)$ are complete elliptic integrals of the first and the second kind, respectively. From (62) it may be shown that the limiting values of $k_1(A)$ and $k_1(B)$ are

$$k_1(A) \to \sigma_0\sqrt{(B-A)/2} \; , \quad k_1(B) \to \sigma_0\sqrt{(B-A)/2} \; . \tag{63}$$

for $(B-A)$ = constants, $B-A \to \infty$, and

$$k_I(B) \to \sigma_0\sqrt{B}\,, \quad k_I(A) \to \infty\,. \tag{64}$$

for $B$ = constant, $A \to 0$. In the latter case noting that $B$ = constant and $k_I(B)$ is a function of $A$, it may also be shown that

$$\lim_{A\to 0} \frac{d}{dA} k_I(B) = -\infty\,, \tag{65}$$

that is, for small values of $A$, $k_I(B)$ is not well defined. The corresponding strain energy release rates at the crack tips A and B are given by

$$\mathcal{G}_A = \frac{\pi k_I^2(A)}{8\mu(1+\kappa)}\,, \quad \mathcal{G}_B = \frac{\pi k_I^2(B)}{8\mu(1+\kappa)}\,. \tag{66}$$

Similarly for $(B-A) \to \infty$ we have the reference value

$$\mathcal{G}_A = \mathcal{G}_B = \mathcal{G}^* = \frac{\pi\sigma_0^2(B-A)/2}{8\mu(1+\kappa)}\,. \tag{67}$$

## 7. Numerical Results and Discussion

For the bonded dissimilar materials with interface cracks from (37)-(39) it is seen that the integral equations are of the second kind (that is $\gamma \neq 0$), and, consequently, the fundamental solution w which controls asymptotic nature of stresses and displacements near the crack tips has complex singularities resulting in the well-known oscillatory stress and displacement behavior. For example, for a single interface crack in two bonded orthotropic half planes under uniform stresses at infinity, from (52) the crack opening displacements may be obtained as

$$u_{12}(x_1,+0)-u_{22}(x_1,-0)=\frac{\sqrt{a^2-x_1^2}}{\sqrt{1-\varepsilon^2}}\left\{\frac{\sigma_0}{\tau_{12}}\cos\left(\varepsilon\log\left(\frac{a+x_1}{a-x_1}\right)\right)\right.$$
$$\left.-\frac{\tau_0}{\sqrt{\tau_{12}\tau_{21}}}\sin\left(\varepsilon\log\left(\frac{a+x_1}{a-x_1}\right)\right)\right\},$$

$$u_{11}(x_1,+0)-u_{21}(x_1,-0)=\frac{\sqrt{a^2-x_1^2}}{\sqrt{1-\varepsilon^2}}\left\{\frac{\tau_0}{\tau_{21}}\cos\left(\varepsilon\log\left(\frac{a+x_1}{a-x_1}\right)\right)\right.$$
$$\left.+\frac{\sigma_0}{\sqrt{\tau_{12}\tau_{21}}}\sin\left(\varepsilon\log\left(\frac{a+x_1}{a-x_1}\right)\right)\right\}. \qquad (68)$$

Equation (68) shows that as $x_1\to\mp a$ the displacements would oscillate leading to an apparent crack surface interference. The bimaterial constant $\varepsilon$ which controls these oscillations is defined by (39) in terms of $\gamma$, which in turn is given by (26)-(28) or (60). It is perhaps worthwhile to emphasize that in crack problems there are really two kinds of crack surface interference. One is the mathematical consequence of the assumed jump discontinuities in material constants across the interface, giving oscillations even under pure mode I loading conditions. However, for practical material pairs the size of this interference region having the forms $\Delta u\sim\sqrt{a-x_1}\cdot\sin(\varepsilon\log(a-x_1))$ or $\Delta u\sim\sqrt{a-x_1}\cdot\cos(\varepsilon\log(a-x_1))$ is usually of the order or smaller than the microstructural length parameters and its effect on the fracture analysis is rather negligible. Furthermore, this behavior may be removed by assuming a more realistic material model in which the jump discontinuities are replaced by "thin" interfacial regions with steeply varying material properties [23].

The second kind of crack surface interference is macroscopic and geometric, and is invariably the consequence of mode II loading in crack problems that lack symmetry with respect to the plane of the crack (e.g., an embedded crack parallel to the interface or the free surface). In the case of an interface crack in bonded dissimilar materials, since the plane of the crack is not a plane of symmetry, under pure mode II loading the normal component of the crack surface opening would be an odd function resulting in

surface interference. As an example, Figure 2 shows the normal component $\Delta v = u_{12}^{+} - u_{22}^{-}$ of the crack opening displacement given (68a) for two bonded dissimilar orthotropic half planes for various relative values of tensile and shear loadings $\sigma_0$ and $\tau_0$. The calculations neglect the interference. Hence along a substantial portion of the crack $\Delta v$ seems to be negative. For various $\sigma_0/\tau_0$ ratios the values $x_0$ for which $\Delta v(x_0) = 0$ are given as follows:

| $\sigma_0/\tau_0$: | 0 | 0.1 | 0.2 | 0.5 | 1.0 |
|---|---|---|---|---|---|
| $x_0/a$: | 0 | -0.60536 | -0.88271 | -0.99693 | -0.99996 |

These results indicate that for small values of $\sigma_0/\tau_0$ the interference is macroscopic, the solution given in this paper is not valid and to obtain the correct solution the problem must be formulated as a crack/contact problem (e. g., [24]). However, these results also show that if the mode I component of the external load is sufficiently high, the possible crack surface interference may safely be neglected.

From (26)-(28) and (39) it may be seen that the crack tip stress and displacement oscillations disappear if $\gamma = 0$ or if

$$\frac{1-\nu_{20}}{E_{20}} = \frac{1-\nu_{10}}{E_{10}}, \tag{69}$$

where the "averaged" material constants $E_{i0}$ and $\nu_{i0}$, $(i = 1, 2)$ are defined by (1) for plane stress and (2) for plane strain conditions. From (69) it also follows that in isotropic incompressible materials $\nu_0 = 1/2$ for plane stress and $\nu_0 = 1$ for plane strain and, therefore, oscillations disappear only under plane strain conditions.

In this study two types of examples are given. In the first some specific materials

are considered in various combinations. The elastic properties of these materials are listed in Table 1. Materials a-c are fiber reinforced structural composites (graphite-epoxy). Except for a 90 degree rotation about the z axis, materials a and b are identical. Material k is a crystalline solid (Topaz) and again material *l* is the same as k except for a 90 degree rotation. Materials d-j are isotropic. The material combinations used in the examples are shown in Table 2. In this table materials $m_1$,..., $m_4$ are assumed to represent the grain boundary region in bonded Topaz crystals. They are assumed to be isotropic having hypothetically selected elastic constants.

Table 3 shows the material combinations used in the second group of examples in which two dissimilar isotropic materials, carbon and epoxy, are assumed to be bonded through an orthotropic interfacial layer of hypothetically selected properties. Depending on the processing and coupling agents used, the interfacial zone may exhibit either a columnar ($E_{222} > E_{211}$) or a lamellar ($E_{222} < E_{211}$) structure ($E_{222}$ and $E_{211}$ being the Young's moduli in $x_2$ and $x_1$ directions, respectively). In each example only one material parameter ($E_{211}$, $E_{222}$ or $G_{212}$) is varied. Since three of the Poisson's ratios are fixed, the remaining three must be varied along with the Young's moduli to maintain the symmetry of the elasticity matrix. The table also shows the oscillation parameter $\omega$ defined by (39) and the strain energy release rates $\mathcal{G}_0$ and $\mathcal{G}_\infty$ corresponding to two half plane solutions obtained from (54) for a single pressurized crack and for $h = 0$ and $h = \infty$, respectively. (Fig. 1).

The results given in this section are obtained under mode I loading $\sigma_0$ and plane strain conditions, and consist of largely the strain energy release rate $\mathcal{G}$ which, in the case of the interface cracks, is accepted to be the main crack driving force. Figures 3 and 4 show some sample results for the material combinations given in Table 2. Examples F through $H_3$ and J correspond to structural applications involving metals

and fiber reinforced composites bonded through an epoxy layer. In I the adherents are silicon carbide and alumina and the interfacial region is amorphous carbon. In examples $H_1$, $H_2$ and $H_3$ the crack is between aluminum (med. 1) and epoxy layer (med. 2) and the third material (med. 3) is a fiber reinforced composite. In all cases the variable is h/2a. Note that for each case the normalizing stress intensity factor $\mathcal{G}_0$ is given in Table 2 and is calculated from (54) (for the corresponding material pairs 1 and 3). The figures show that $\mathcal{G}/\mathcal{G}_0$ approaches 1 for (h/2a)—0 and $\mathcal{G}_\infty/\mathcal{G}_0$ for (h/2a)—$\infty$ (the latter limit is also given in Table 2). Also, since the stiffness of the interfacial layer is less than that of the medium 3, $\mathcal{G}$ is in all cases a monotonically increasing function of h/2a.

Figures 5 and 6 show the strain energy release rate for material combinations $K_1$,... $K_4$ defined in Table 2. Again $\mathcal{G}_0$ corresponds to $h = 0$. Note that in case $K_4$ since the stiffness of medium 2 is greater than that of medium 3 we have $\mathcal{G}_0 > \mathcal{G}_\infty$.

The results for the second group of examples A through E described in Table 3 are shown in Figures 7-13. The parameter $e$ shown in the figures corresponds to the ratios $E_{211}/E_3$, $E_{222}/E_3$ or $G_{212}/G_3$ and represents the structure of the interfacial zone. Here again $\mathcal{G}_0$ is the strain energy release rate corresponding to $h = 0$, that is, to the material pair 1 and 3. Note that the crack is between materials 1 and 2 and consequently, as seen from the figures, $\mathcal{G} > \mathcal{G}_0$ if the stiffness of the interfacial region is less than that of medium 3, i.e., for $e < 1$ and $\mathcal{G} < \mathcal{G}_0$ for $e > 1$. Also, in all cases except in case B $\mathcal{G}$ is bounded by $\mathcal{G}_0$ and $\mathcal{G}_\infty$. Figure 13 shows the influence of the modulus ratio $e$ on the strain energy release rate for $h/2a = 0.4$. For $e = 1$ materials 2 and 3 are identical and $\mathcal{G} = \mathcal{G}_0$. The figure shows that as expected $\mathcal{G}/\mathcal{G}_0$ is a monotonically decreasing function of $e$. The exception is again Case B in which the modulus $E_{211}$ parallel to the interface seems to have very little influence on $\mathcal{G}$. This result may also be observed in Figure 8.

The results for the collinear cracks obtained under plane strain conditions and

uniform tension $\sigma_0$ are shown in Figures 14-20. In all these Figures the normalizing strain energy release rate $\mathcal{G}^*$ is obtained for a single crack of length 2a and for the particular material or material combination with the given h/2a ratios. Figures 14 and 15 show the results for an isotropic homogeneous plane (full lines) and two dissimilar isotropic half planes (dashed lines) containing two interface cracks of lengths 2a and 2c. The properties of the dissimilar half planes ($E_1 = 1$ GPA, $E_2 = 15$ GPA, $\nu_1 = \nu_2 = 0.1$) are selected to give an unusually large oscillation parameter ($\varepsilon = -0.1306$). In both cases the limiting values of the normalized strain energy release rates are

$$\mathcal{G}_A/\mathcal{G}^* = \mathcal{G}_B/\mathcal{G}^* = 1\ ,\ \mathcal{G}_C/\mathcal{G}^* = \mathcal{G}_D/\mathcal{G}^* = c/a\ ,\ \text{for } d/a \to \infty\ ,$$

$$\mathcal{G}_A \to \infty\ ,\ \mathcal{G}_D \to \infty\ ,\quad \mathcal{G}_B/\mathcal{G}^* = \mathcal{G}_C/\mathcal{G}^* = (c+a)/a\ ,\ \text{for } d/a = 0\ , \tag{70}$$

where d is the distance between the inner crack tips D and A and the subscripts C, D, A and B refer to the crack tips shown in the figures. c = a in the example shown in Fig. 14 and c = 0.2a in Fig. 15. For the dissimilar materials considered we have $\mathcal{G}^* = 1.50363\ \sigma_0^2 a\ (\text{GPA})^{-1}$. A rather interesting and very useful result shown by Figures 14 and 15 is that the normalized strain energy release rates for the collinear cracks in bonded materials may be approximated by that obtained from a homogeneous isotropic medium having the same crack geometry. For the latter very often it is possible to obtain a closed form solution (see, for example, equations (62) and (66) which were used to plot the solid curves in Fig. 14).

Figures 16-20 show the normalized strain energy release rates in bonded orthotropic materials (material combination G, Table 2) containing two collinear interface cracks with c/a = 1, 0.5, 0.2, 0.1 and 0.05, respectively. In these figures solid

lines again correspond to the homogeneous isotropic plane with the same crack geometry as the bonded planes. The round dots give the results for two half planes ($h = \infty$, materials a and d) and the square dots for two half planes (materials a and c) bonded through a layer (material d) with $h/2a = 1$. It may be seen that $\mathcal{G}/\mathcal{G}^*$ ratios for the two dissimilar half planes are nearly identical to the isotropic plane values. There is, however, some discrepancy between the isotropic plane and the interfacial layer results. Table 4 shows the limiting values of $\mathcal{G}/\mathcal{G}^*$ given in Figures 16-20 for $d/a \to 0$ and $d/a \to \infty$. Note that for $h/2a = \infty$ the limits for homogeneous isotropic and bonded orthotropic materials are identical, whereas for $h/2a = 1$ both limits differ from the homogeneous plane results. Despite this considering the additional difficulties involved in solving the multiparameter problem of collinear cracks in bonded materials, the discrepancies may be tolerable. For the material combination G and for various h/2a ratios the value of $\mathcal{G}^*$ are given in Table 5. Some additional results for the collinear cracks for a fixed d ($d/a = 0.1$) and varying values of h/2a may be found in Table 6.

Some sample results for the stress intensity factors along with the corresponding strain energy release rates are given in Tables 7 and 8. Equations (48) show that aside from the material constants and the length parameters, the stress intensity factors depend on the dimensionless quantities $g_k(\mp 1)$ defined in (40). In the examples considered the external load is uniform tension $\sigma_{22} = \sigma_0$ at infinity. Thus, the dimensionless quantities $F/\sigma_0$ given in Tables 7 and 8 to represent the stress intensity factors at the crack tips $a_1$, $b_1$, $a_2$, $b_2$ (Fig. 1) or C, D, A, B (Fig. 17) are defined by

$$F(C) = \gamma_{21}\sqrt{1-\gamma^2}\; g_1(-1), \quad F(D) = -\gamma_{21}\sqrt{1-\gamma^2}\; g_1(1),$$

$$F(A) = \gamma_{21}\sqrt{1-\gamma^2}\; g_2(-1), \quad F(B) = -\gamma_{21}\sqrt{1-\gamma^2}\; g_2(1). \tag{71}$$

Note that $\gamma$ is dimensionless and $\gamma_{21}$ has the dimension of stress. The material combination G is again used in the examples (see Tables 1 and 2) for which we have $\gamma_{21} = 1.8098$ GPA, $\gamma_{12} = 1.7684$ GPA, $\omega = 0.071765$. From (48) and (71) one may also note that the stress intensity factors are proportional to $\sqrt{(b_k - a_k)/2}$ as well as F. Thus for $c/a = 0.2$ despite the seemingly high values of F(D) given in Table 7, from a fracture propagation view point by far the worst location is the crack tip A. This may be seen from the values of the strain energy release rates for which the same normalization constants, $\sigma^2 a$ is used in all crack tips. In the case of collinear cracks, as may be seen from Figures 15 and 17-20, this conclusion appears to be quite general meaning that, for example, under cyclic loading fastest subcritical crack growth would take place at the crack tip A. Also it appears that for small values of d/a $\mathcal{G}_C < \mathcal{G}_B < \mathcal{G}_D < \mathcal{G}_A$, whereas for greater d/a one would have $\mathcal{G}_C < \mathcal{G}_D < \mathcal{G}_B < \mathcal{G}_A$. This may have bearing on the crack nucleation, growth and coalescence ahead of a main crack in creep, corrosion as well as fatigue crack growth studies.

Acknowledgements. This work was supported under Office of Naval Research Contract N00014-89-J3188.

References

1. Hutchinson, J. W. and Suo, Z., in J. W. Hutchinson and T. Y. Wu. (eds), *Advances in Applied Mechanics*, 1991.
2. Rice, J. R.; Suo, Z. and Wang, J. S., in M. Ruhle, A. G. Evans, M. F. Ashley and J. Hirth (eds), *Metal Ceramic Interfaces*, Pergamon Press, 1990, p. 169.
3. Erdogan, F., *J. Eng. Fracture Mechanics, Vol. 4* (1972) 811.
4. Manson, J. J., *Pure and Applied Chemistry, Vol. 57* (1985) 1667.
5. Erdogan, F. and Gupta, G. D., *Int. J. Solids Structures, Vol. 7* (1971) 39.

6. Erdogan, F. and Gupta, G. D., *Int. J. Solids Structures, Vol. 7* (1971) 1089.

7. Arin, K. and Erdogan, F., *Int. J. Eng. Sci., Vol. 9* (1971) 213.

8. Erdogan, F. and Arin, K., *Int. J. Eng. Sci., Vol. 10* (1972) 115.

9. Ishida, H., *Polymer Composites, Vol. 5* (1984) 101.

10. Gotoh, M., *Int. J. Fracture Mech., Vol. 3* (1967) 253.

11. Clements, D. L., *Int. J. Eng. Sci., Vol. 9* (1971) 257.

12. Ting, T. C. T., *Int. J. Solids Structures, Vol. 22* (1986) 965.

13. Suo, Z., *Proc. Roy. Soc. Lond. A427* (1990) 331.

14. Bassani, J. L. and Qu, J., *J. Mech. Phys. Solids, Vol.37* (1989) 435.

15. Qu., J. and Bassani, J. L., *J. Mech. Phys. Solids, Vol. 37* (1989) 417.

16. Delale, F. and Erdogan, F., *Int. J. of Fracture, Vol. 15* (1979) 343.

17. Krenk, S., *J. of Composite Materials, Vol. 13* (1979) 108.

18. Cinar, A. and Erdogan, F., *Int. J. of Fracture, Vol. 23* (1983) 83.

19. Chou, Y. T., *J. of Appl. Phys., Vol. 33* (1962) 2747.

20. Erdogan, F. and Wu, B., Submitted for publication, *J. Mech. Phys. Solids*, (1992).

21. Erdogan, F., in S. Nemat-Nasser (ed.), *Mechanics Today, Vol. 4*, Pergamon Press, 1978, p.1.

22. Erdogan, F., *Proc. 4th. U.S. National Congress of Applied Mechanics*, (1962) 547.

23. Delale, F. and Erdogan, F., *Int. J. Eng. Sci., Vol. 26* (1988) 559.

24. Comninou, M., *J. of Appl. Mech., Vol. 44* (1977) 631.

Table 1. The elastic constants of materials used in the examples (moduli in units of GPA.)

| | Mat. a | Mat. b | Mat. c | Mat. k | Mat. *l* |
|---|---|---|---|---|---|
| $E_x$ | 153.09 | 40.403 | 30.6 | 282.486 | 225.734 |
| $E_y$ | 40.405 | 153.09 | 39.0 | 225.734 | 282.486 |
| $E_z$ | 22.754 | 22.754 | 6.4 | 261.097 | 261.097 |
| $G_{xy}$ | 29.304 | 29.304 | 19.7 | 131.06 | 131.06 |
| $G_{yz}$ | 1.551 | 4.082 | 4.5 | 132.98 | 108.11 |
| $G_{xz}$ | 4.082 | 1.551 | 4.5 | 108.11 | 132.98 |
| $\nu_{xy}$ | 1.834 | 0.484 | 0.351 | 0.312 | 0.312 |
| $\nu_{xz}$ | 0.195 | 0.261 | 0.275 | 0.244 | 0.149 |
| $\nu_{yz}$ | 0.261 | 0.195 | 0.275 | 0.149 | 0.244 |

| Material | E | $\nu$ | Material | E | $\nu$ |
|---|---|---|---|---|---|
| d (epoxy) | 3.1 | 0.35 | j (high modulus carbon) | 380 | 0.32 |
| e (aluminum) | 69 | 0.3 | $m_1$ | 2.5 | 0.3 |
| f (steel) | 200 | 0.3 | $m_2$ | 25 | 0.3 |
| g (amorphous carbon) | 8.3 | 0.32 | $m_3$ | 250 | 0.3 |
| h (silicon carbide) | 207 | 0.2 | $m_4$ | 1000 | 0.3 |
| i (alumina) | 325 | 0.3 | | | |

Table 2. Material Combinations F-$K_4$ used in the examples. $\sigma$ is the uniform crack surface pressure and 2a is the crack length. (see Fig. 1 for geometry and Table 1 for the properties of materials a-$l$)

| Mat. Comb. | Med. 1 | Med. 2 | Med. 3 | $\mathcal{G}_0/\sigma^2 a$ $(GPA)^{-1}$ | $\mathcal{G}_\infty/\sigma^2 a$ $(GPA)^{-1}$ | $\mathcal{G}_\infty/\mathcal{G}_0$ | $\omega$ | Fig. |
|---|---|---|---|---|---|---|---|---|
| F | a | d | b | 0.0343 | 0.4532 | 13.2 | 0.0718 | 3 |
| G | a | d | c | 0.0569 | 0.4532 | 7.966 | 0.0718 | 3 |
| H | a | d | e | 0.0427 | 0.4532 | 10.62 | 0.0718 | 3 |
| $H_1$ | e | d | a | 0.0427 | 0.4531 | 10.62 | 0.0671 | 4 |
| $H_2$ | e | d | b | 0.0320 | 0.4531 | 14.14 | 0.0671 | 4 |
| $H_3$ | e | d | c | 0.0565 | 0.4531 | 8.027 | 0.0671 | 4 |
| I | h | g | i | 0.0116 | 0.1722 | 14.88 | 0.0843 | 3 |
| J | e | d | f | 0.0273 | 0.4531 | 16.61 | 0.0671 | 3 |
| $K_1$ | k | $m_1$ | $l$ | 0.0109 | 0.5501 | 50.54 | 0.0471 | 5 |
| $K_2$ | k | $m_2$ | $l$ | 0.0109 | 0.0605 | 5.60 | 0.0741 | 5 |
| $K_3$ | k | $m_3$ | $l$ | 0.0109 | 0.0165 | 1.06 | -0.0105 | 6 |
| $K_4$ | k | $m_4$ | $l$ | 0.0109 | 0.007 | 0.645 | -0.0749 | 6 |

Table 3. Material combinations A-E used in the examples. Referring to Fig. 1 and Table 1, medium 3 is epoxy (d) in all cases; medium 1 is amorphous carbon (g) in A-E and high modulus carbon (j) in case $D_1$. The moduli of medium 2 are selected as shown: the Poisson's ratios are given by $\nu_{212} = \nu_{231} = \nu_{232} = 0.35 = \nu_3$. The external load is uniform crack surface pressure $\sigma$ and the crack length is 2a.

| Case | $\frac{E_{211}}{E_3}$ | $\frac{E_{222}}{E_3}$ | $G_{212}$ | $\mathcal{G}_0/\sigma^2 a$ $(GPA)^{-1}$ | $\mathcal{G}_\infty/\sigma^2 a$ $(GPA)^{-1}$ | $\mathcal{G}_\infty/\mathcal{G}_0$ | $\omega$ | Fig. |
|---|---|---|---|---|---|---|---|---|
| A | 1 | 1/4 | $G_3$ | 0.6139 | 0.8622 | 1.404 | 0.0333 | 7, 13 |
| | 1 | 4 | $G_3$ | 0.6139 | 0.3822 | 0.623 | -0.0196 | |
| B | 1/4 | 1 | $G_3$ | 0.6139 | 0.6056 | 0.986 | 0.0128 | 8, 13 |
| | 4 | 1 | $G_3$ | 0.6139 | 0.5791 | 0.943 | -0.0129 | |
| C | 1/4 | 1 | $\frac{E_{211}}{2(1+\nu_3)}$ | 0.6139 | 0.9745 | 1.587 | 0.0017 | 9, 13 |
| | 4 | 1 | | 0.6139 | 0.3995 | 0.651 | -0.0115 | |
| D | 1 | 1/4 | $\frac{E_{222}}{2(1+\nu_3)}$ | 0.6139 | 1.4111 | 2.299 | 0.0208 | 10, 13 |
| | 1 | 4 | | 0.6139 | 0.2849 | 0.464 | -0.0276 | |
| E | 1 | 1 | $1/4\ G_3$ | 0.6139 | 0.9792 | 1.594 | 0.0173 | 12, 13 |
| | 1 | 1 | $4G_3$ | 0.6139 | 0.4576 | 0.745 | 0.0370 | |
| $D_1$ | 1 | 1/4 | $\frac{E_{222}}{2(1+\nu_3)}$ | 0.4344 | 1.2349 | 2.842 | 0.0396 | 11, 13 |
| | 1 | 4 | | 0.4344 | 0.1167 | 0.269 | 0.0383 | |

Table 4. The limiting values of the strain energy release rates shown in Figures 16-20. $\mathcal{G}_{orth.}$ corresponds to material combination G given in Table 2. Loading is uniform tension $\sigma_0$. $(\mathcal{G}^*)_{iso.} = (1+\kappa)\sigma_0^2 a/8\mu$. $(\mathcal{G}^*)_{orth.} = 0.45320\sigma_0^2 a$ $(\mathrm{GPA})^{-1}$ and $(\mathcal{G}^*)_{orth.} = 0.41108\ \sigma_0^2 a\ (\mathrm{GPA})^{-1}$ are the single crack values, for a homogeneous medium, for two dissimilar half planes (materials a and d), and for two half planes bonded through a layer (mat. comb. G, h/2a = 1), respectively.

| | | | c/a | | | | |
|---|---|---|---|---|---|---|---|
| d/a | h/2a | $\mathcal{G}/\mathcal{G}^*$ | 1 | 0.5 | 0.2 | 0.1 | 0.05 |
| $\infty$ | – | $(\mathcal{G}_{\ell}/\mathcal{G}^*)_{iso.}$ | 1 | 0.5 | 0.2 | 0.1 | 0.05 |
| $\infty$ | 1 | $(\mathcal{G}_{\ell}/\mathcal{G}^*)_{orth.}$ | 1 | 0.535 | 0.219 | 0.110 | 0.055 |
| 0 | – | $(\mathcal{G}_{B,\ell}/\mathcal{G}^*)_{iso.}$ | 2 | 1.5 | 1.2 | 1.1 | 1.05 |
| 0 | 1 | $(\mathcal{G}_{B,\ell}/\mathcal{G}^*)_{orth.}$ | 1.694 | 1.372 | 1.166 | 1.083 | 1.041 |
| $\infty$ | $\infty$ | $(\mathcal{G}_{\ell}/\mathcal{G}^*)_{orth.}$ | 1 | 0.5 | 0.2 | 0.1 | 0.05 |
| 0 | $\infty$ | $(\mathcal{G}_{B,\ell}/\mathcal{G}^*)_{orth.}$ | 2 | 1.5 | 1.2 | 1.1 | 1.05 |

Table 5. Values of $\mathcal{G}^*$ for the material combination G. (Table 3)

| h/2a | $\infty$ | 10 | 4 | 2 | 1 | 0.5 | 0 |
|---|---|---|---|---|---|---|---|
| $\mathcal{G}^*/\sigma_0^2 a\ (\mathrm{GPA})^{-1}$ | 0.453 | 0.453 | 0.450 | 0.440 | 0.411 | 0.348 | 0.057 |

Table 6. Strain energy release rates for two orthotropic half planes bonded through a layer of thickness h (material combination G) and containing two collinear cracks of lengths 2a and 2c. d/a = 0.1, d being the distance between the inner crack tips D and A. (Fig. 17)

| | | h/2a | | | | | | |
|---|---|---|---|---|---|---|---|---|
| c/a | | ∞ | 10 | 4 | 2 | 1 | 0.5 | 0 |
| 1 | $G_A/\sigma^2 a(GPA)^{-1}$ | 1.489 | 1.483 | 1.457 | 1.374 | 1.142 | 0.959 | 0.187 |
| 1 | $G_B/\sigma^2 a(GPA)^{-1}$ | 0.605 | 0.603 | 0.592 | 0.561 | 0.484 | 0.399 | 0.076 |
| 0.1 | $G_A/\sigma^2 a(GPA)^{-1}$ | 0.533 | 0.531 | 0.528 | 0.512 | 0.456 | 0.379 | 0.067 |
| 0.1 | $G_B/\sigma^2 a(GPA)^{-1}$ | 0.459 | 0.458 | 0.455 | 0.444 | 0.414 | 0.349 | 0.058 |
| 0.1 | $G_D/\sigma^2 a(GPA)^{-1}$ | 0.209 | 0.208 | 0.206 | 0.206 | 0.191 | 0.168 | 0.026 |
| 0.1 | $G_C/\sigma^2 a(GPA)^{-1}$ | 0.135 | 0.135 | 0.134 | 0.134 | 0.126 | 0.110 | 0.017 |

Table 7. Stress intensity factors and the strain energy release rates in orthotropic half planes bonded through an isotropic layer and containing two collinear interface cracks of length 2a and 2c. c/a = 0.2, h/2a = 1, material combination G. The values of $\mathcal{G}/\sigma_0^2 a$ given are in units of $(GPA)^{-1}$.

| d/a | $F(B)/\sigma_0$ | $\mathcal{G}_B/\sigma_0^2 a$ | $F(A)/\sigma_0$ | $\mathcal{G}_A/\sigma_0^2 a$ |
|---|---|---|---|---|
| $\infty$ | 0.958 – 0.172 $i$ | 0.411 | 0.958 – 0.172 $i$ | 0.411 |
| 4 | 0.960 – 0.172 $i$ | 0.412 | 0.961 – 0.172 $i$ | 0.414 |
| 2 | 0.961 – 0.172 $i$ | 0.413 | 0.961 – 0.172 $i$ | 0.414 |
| 1 | 0.961 – 0.173 $i$ | 0.414 | 0.962 – 0.173 $i$ | 0.415 |
| 0.5 | 0.962 – 0.175 $i$ | 0.415 | 0.985 – 0.176 $i$ | 0.434 |
| 0.1 | 0.970 – 0.178 $i$ | 0.422 | 1.105 – 0.203 $i$ | 0.547 |

| d/a | $F(D)/\sigma_0$ | $\mathcal{G}_D/\sigma_0^2 a$ | $F(C)/\sigma_0$ | $\mathcal{G}_C/\sigma_0^2 a$ |
|---|---|---|---|---|
| $\infty$ | 0.958 – 0.172 $i$ | 0.082 | 0.958 – 0.172 $i$ | 0.082 |
| 4 | 1.035 – 0.149 $i$ | 0.095 | 1.034 – 0.149 $i$ | 0.095 |
| 2 | 1.072 – 0.156 $i$ | 0.102 | 1.056 – 0.154 $i$ | 0.100 |
| 1 | 1.179 – 0.173 $i$ | 0.123 | 1.154 – 0.167 $i$ | 0.118 |
| 0.5 | 1.332 – 0.206 $i$ | 0.158 | 1.271 – 0.186 $i$ | 0.143 |
| 0.1 | 2.053 – 0.378 $i$ | 0.379 | 1.560 – 0.245 $i$ | 0.216 |

Table 8. Stress intensity factors and strain energy release rates in orthotropic half planes bonded through an isotropic layer and containing two collinear cracks of equal length 2a, material combination G. The values of $\mathcal{G}/\sigma_0{}^2a$ given are in units of $(GPA)^{-1}$.

| | d/a = 0.1 | | | | d/a = ∞ | |
|---|---|---|---|---|---|---|
| h/2a | $F(B)/\sigma_0$ | $\mathcal{G}_B/\sigma_0{}^2a$ | $F(A)/\sigma_0$ | $\mathcal{G}_A/\sigma_0{}^2a$ | $F(B)/\sigma_0{}^2a$ | $\mathcal{G}_B/\sigma_0{}^2a$ |
| ∞ | $1.170-0.153i$ | 0.605 | $1.834-0.252i$ | 1.489 | $1.012-0.145i$ | 0.453 |
| 10 | $1.167-0.174i$ | 0.603 | $1.813-0.357i$ | 1.483 | $1.011-0.145i$ | 0.453 |
| 4 | $1.154-0.178i$ | 0.592 | $1.796-0.363i$ | 1.457 | $1.008-0.147i$ | 0.450 |
| 2 | $1.121-0.194i$ | 0.561 | $1.737-0.383i$ | 1.372 | $0.996-0.151i$ | 0.440 |
| 1 | $1.036-0.203i$ | 0.484 | $1.566-0.422i$ | 1.142 | $0.958-0.170i$ | 0.411 |
| 0.5 | $1.018-0.207i$ | 0.399 | $1.429-0.408i$ | 0.959 | $0.873-0.202i$ | 0.348 |

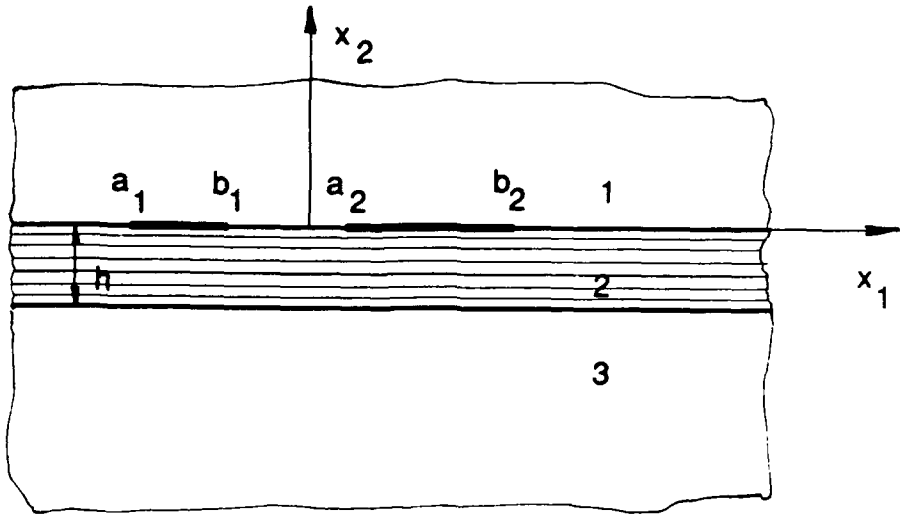


Fig. 1 The geometry of bonded materials with collinear interface cracks.

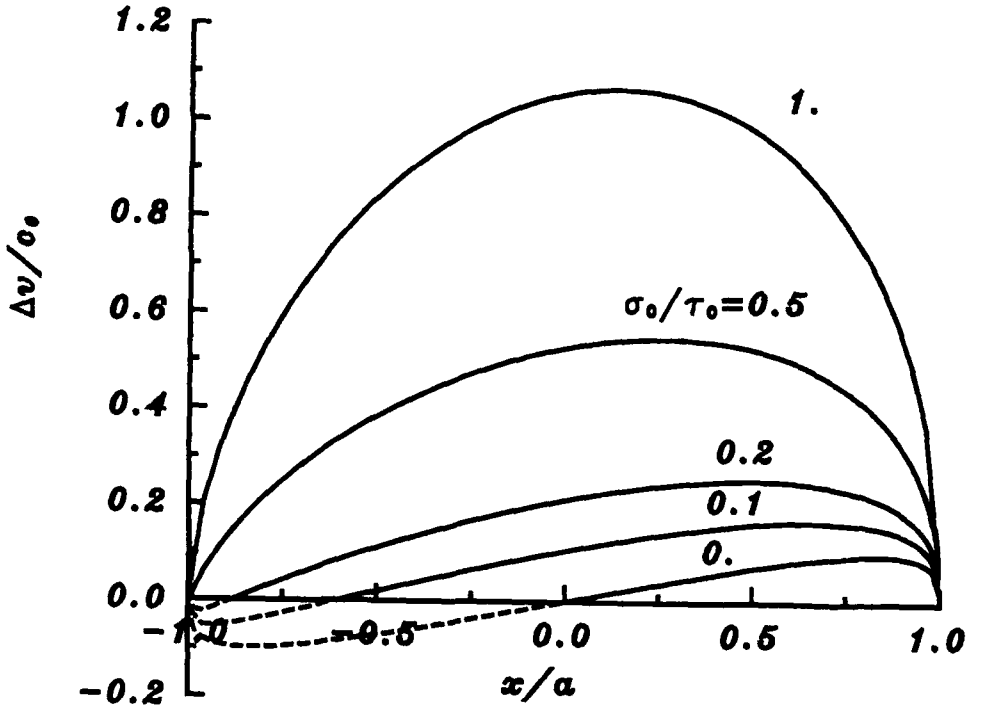


Fig. 2 Normal component of the crack opening displacement $\Delta v = u_{12}{}^{+} - u_{22}{}^{-}$ for an interface crack in two bonded orthotropic half spaces for various values of $\sigma_0/\tau_0$. $\sigma_0$ and $\tau_0$ are respectively the normal and shear components of crack surface tractions. Medium 1 is material c, medium 2 is material a (Table 1), $c_0 = a\tau_0/[\gamma_{12}\gamma_{21}(1-\gamma^2)]^{1/2}$, $\omega = -0.07505$, $\eta = \sqrt{\gamma_{21}/\gamma_{12}} = 1.057$.

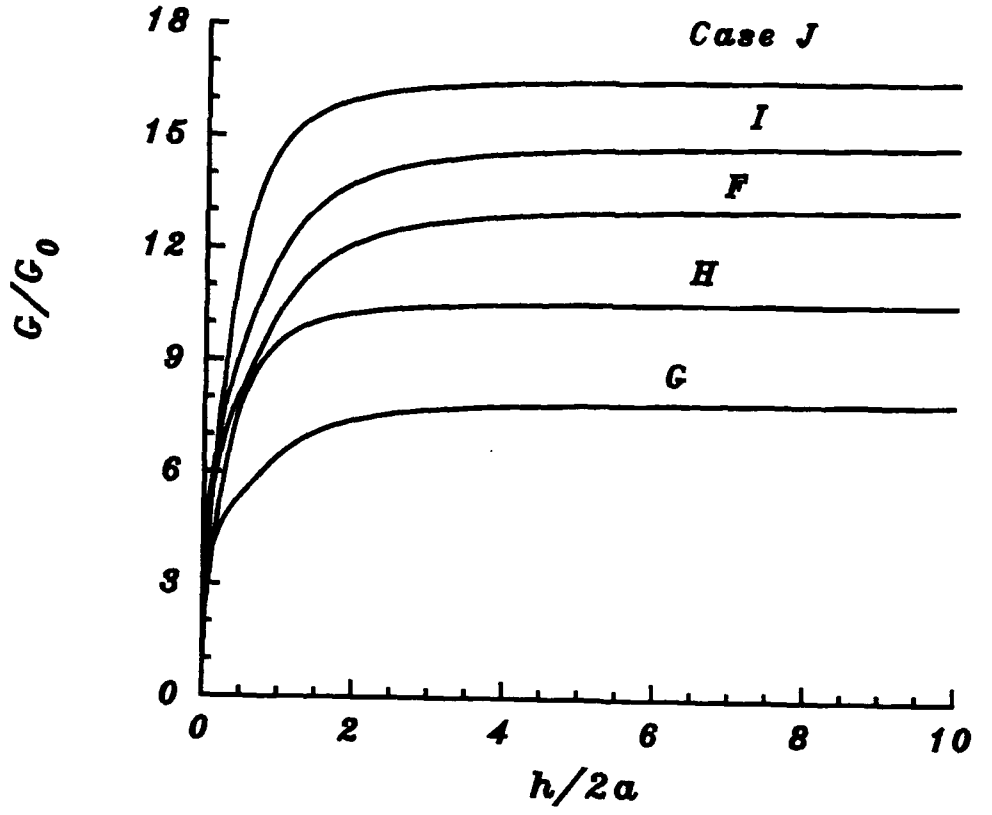


Fig. 3 Strain energy release rate for a single pressurized interface crack in two half planes bonded through a layer. In all cases $\mathcal{G}/\mathcal{G}_0 = 1$ for $h = 0$.

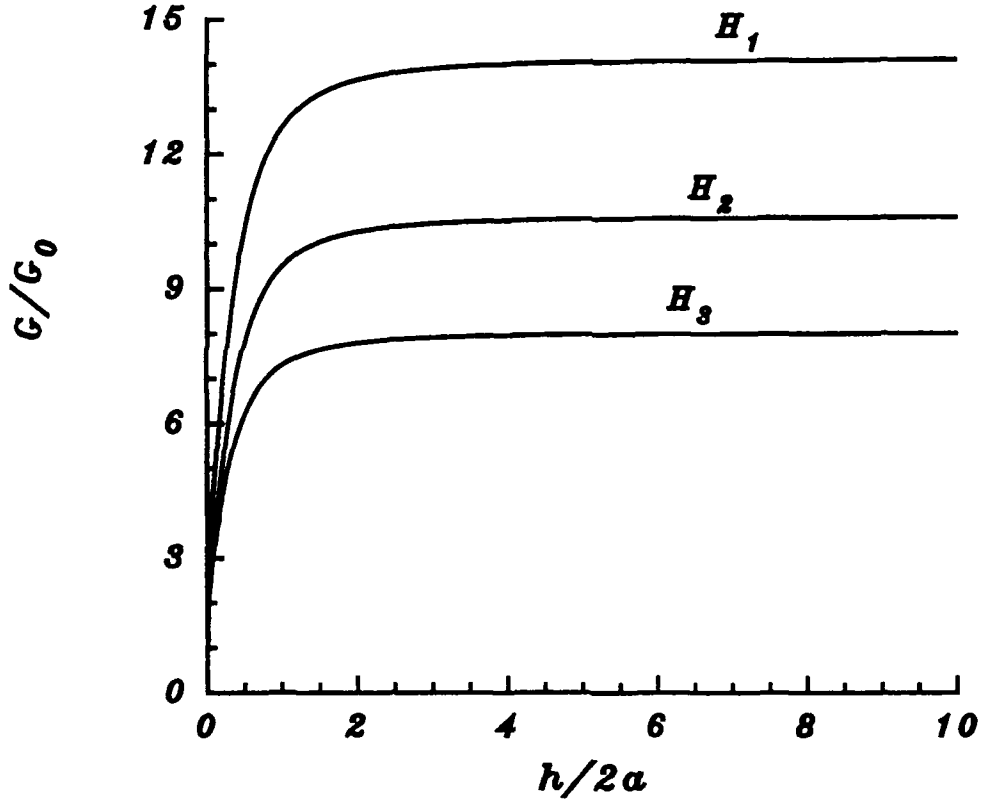


Fig. 4 Same as Fig. 3 for material combinations $H_1$, $H_2$ and $H_3$.

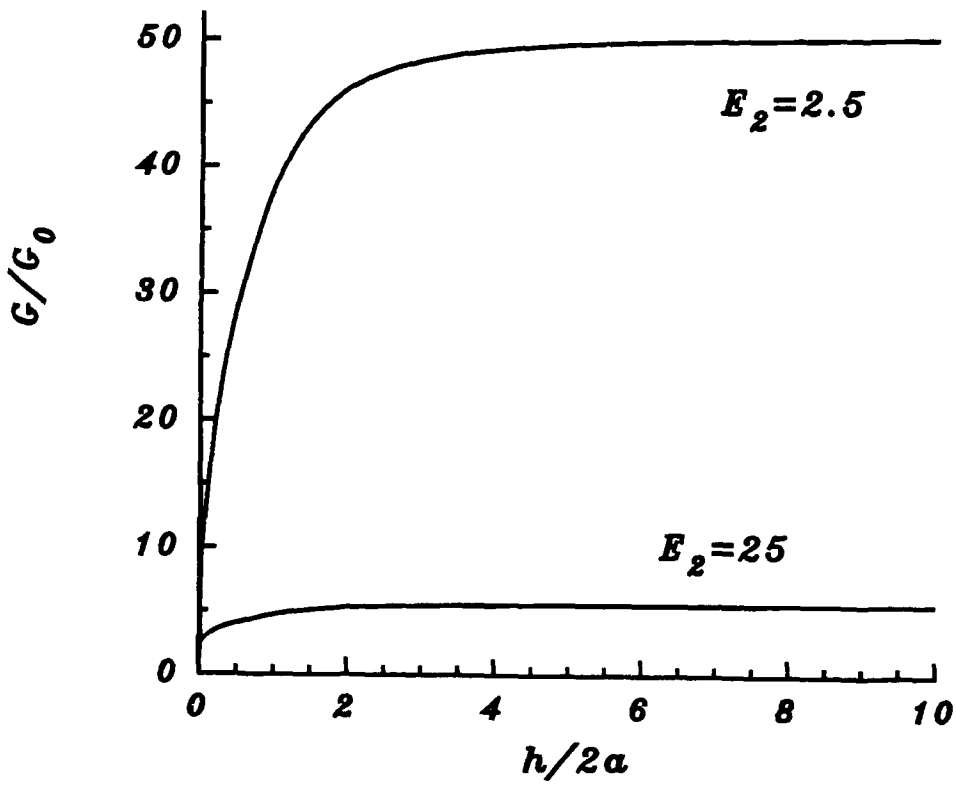


Fig. 5 Strain energy release rate in two orthotropic half planes bonded through an isotropic layer and containing a pressurized crack. Material combinations $K_1$ and $K_2$ (Table 2). $\mathcal{G}/\mathcal{G}_0 = 1$ for $h/2a = 0$.

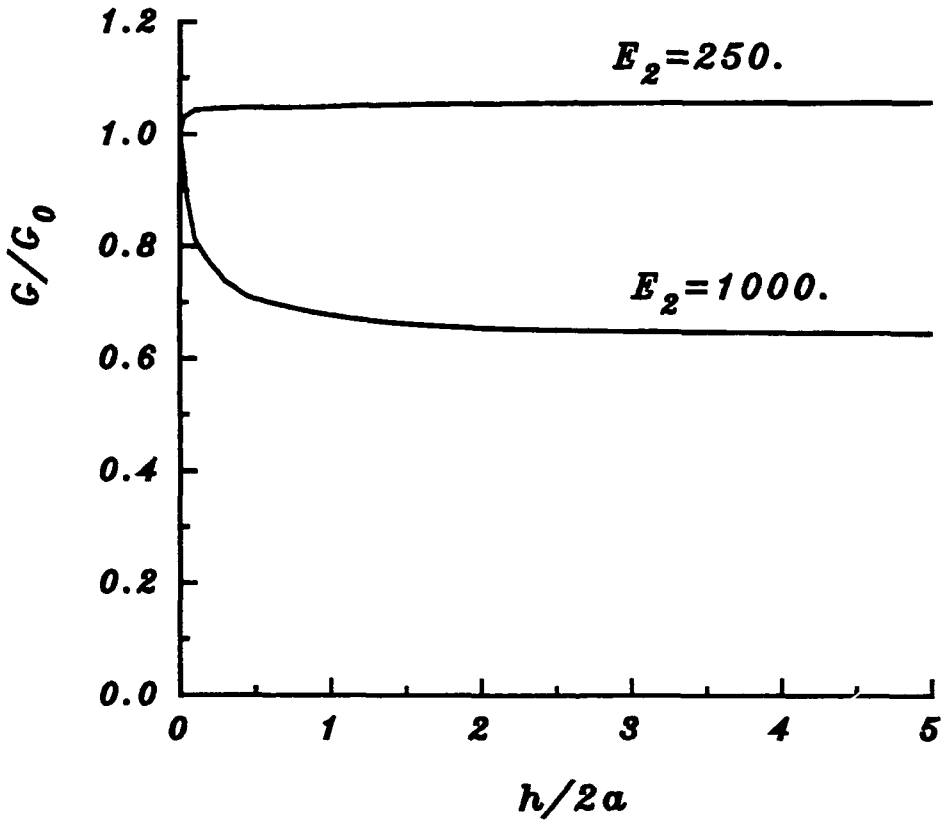


Fig. 6 Same as Fig. 5, material combinations $K_3$ and $K_4$ (Table 2).

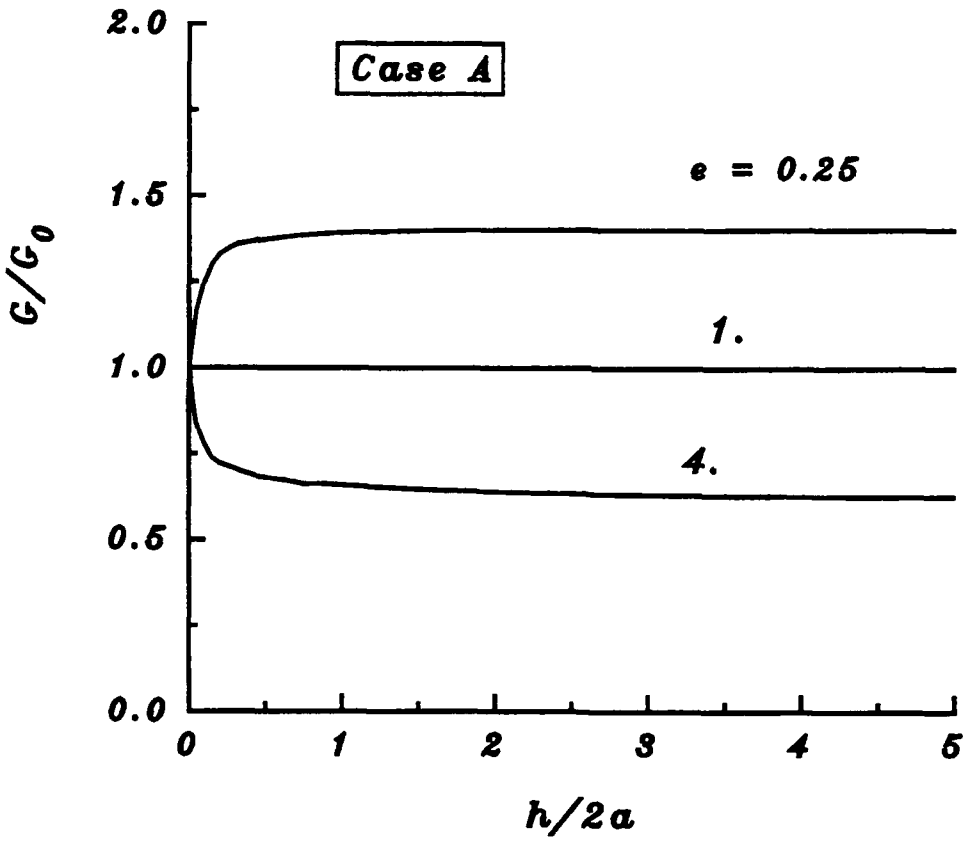


Fig. 7 Strain energy release rates in two isotropic half planes bonded through an orthotropic layer and containing a pressurized interface crack. Material combination A (Table 3), $G_{212} = G_3$, $e = E_{222}/E_3$.

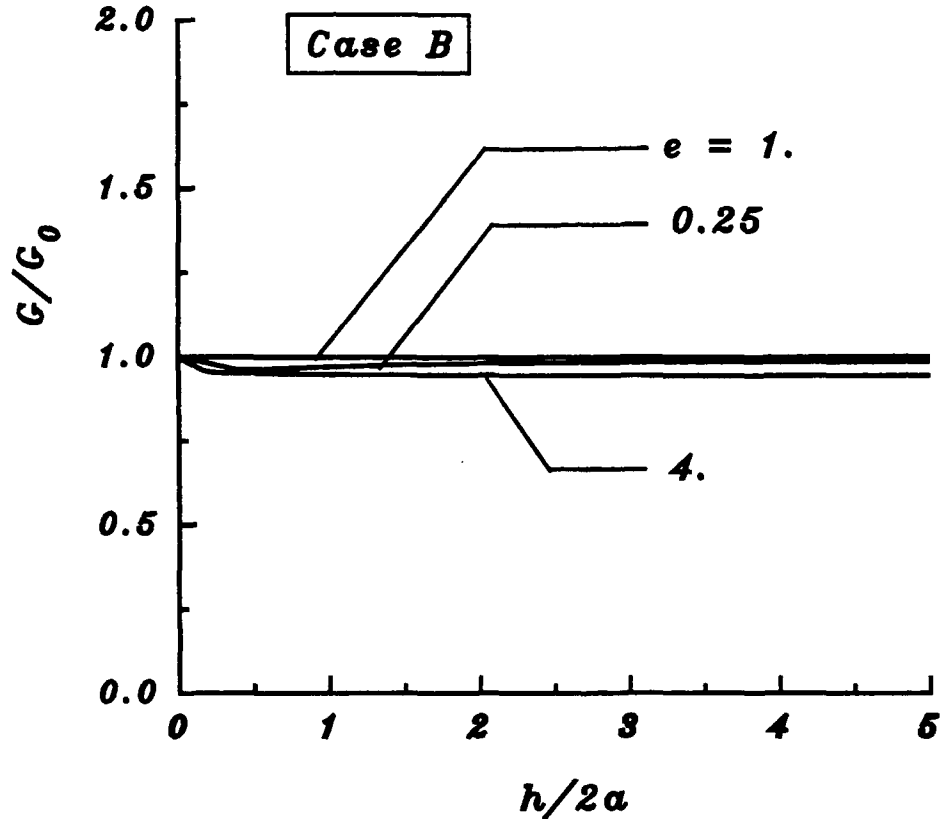


Fig. 8 Same as Fig. 7, material combination B. $e = E_{211}/E_3$. $G_{212} = G_3$.

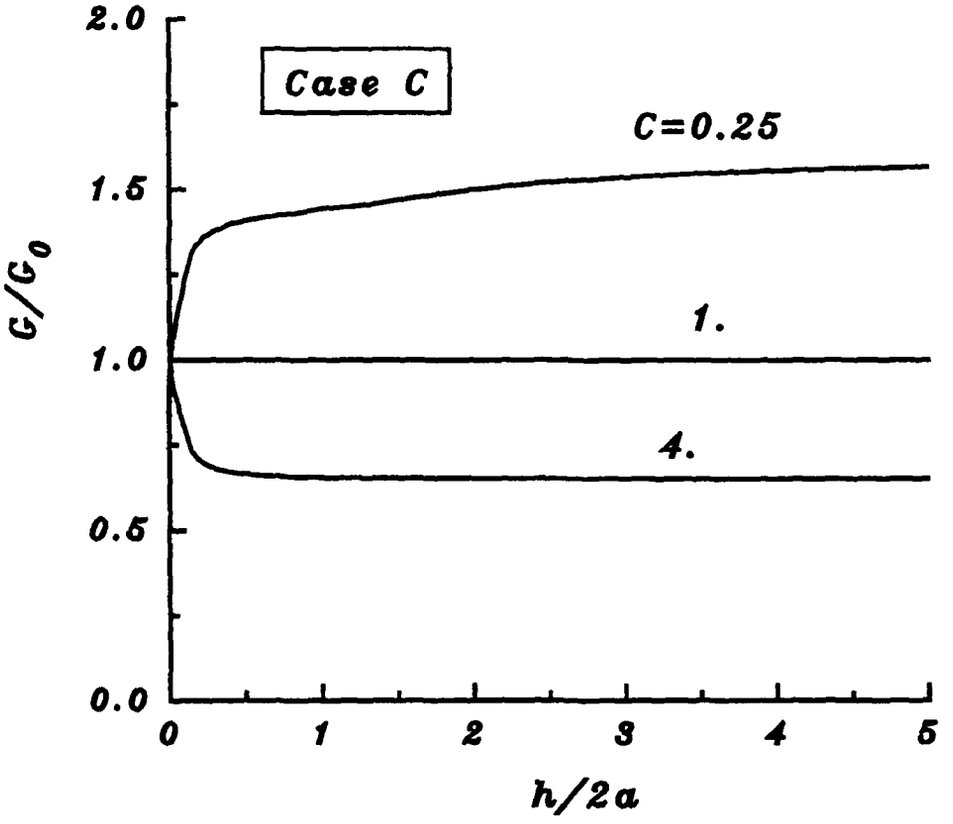


Fig. 9 Same as Fig. 7, material combination C. $e = E_{211}/E_3$, $G_{212} = E_{211}/2(1+\nu_3)$.

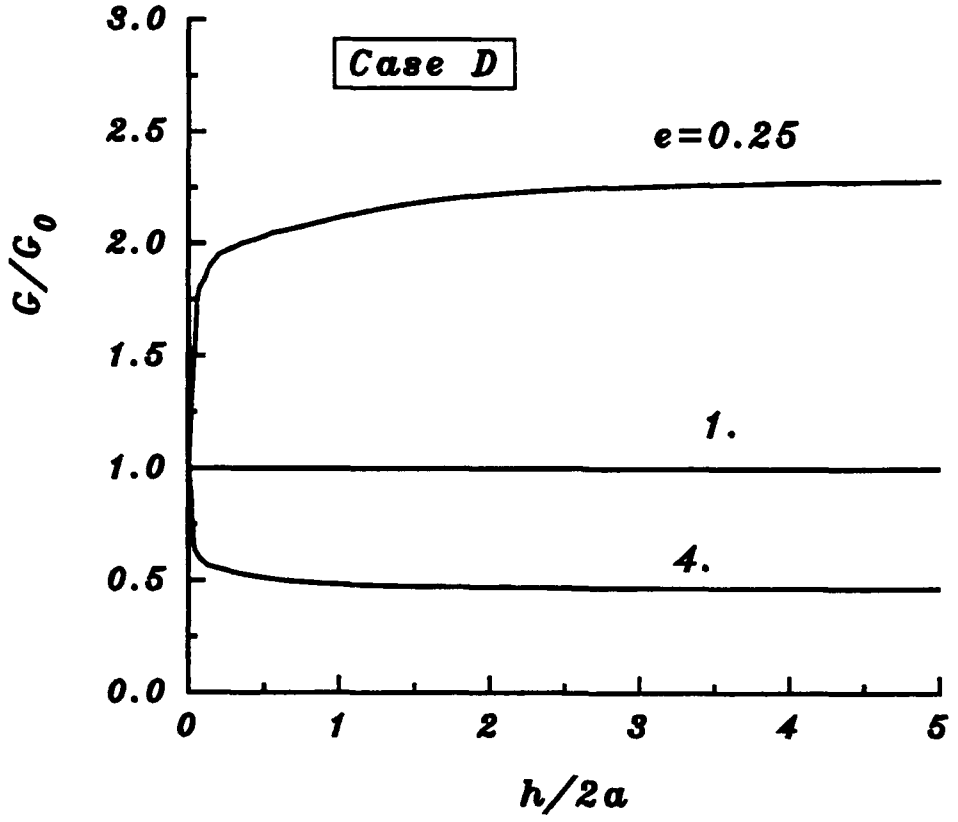


Fig. 10 Same as Fig. 7, material combination D, $e = E_{222}/E_3$, $G_{212} = E_{222}/2(1+\nu_3)$.

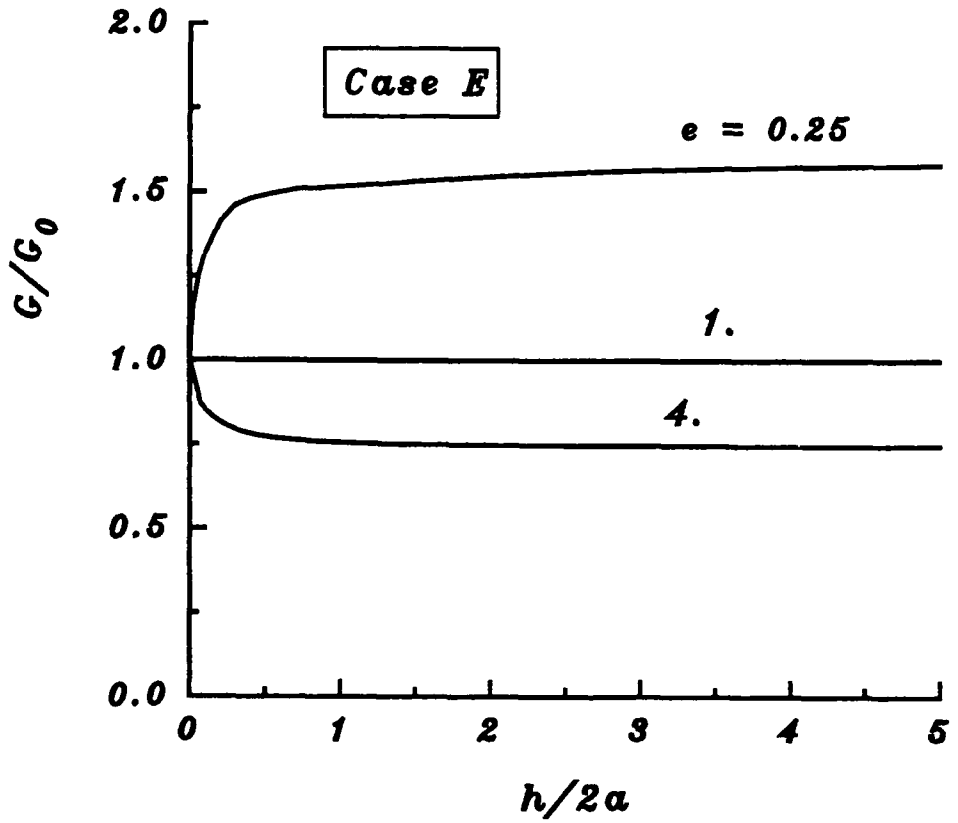


Fig. 11 Same as Fig. 7 material combination E, $e = G_{212}/G_3$, $E_{211} = E_{222} = E_3$.

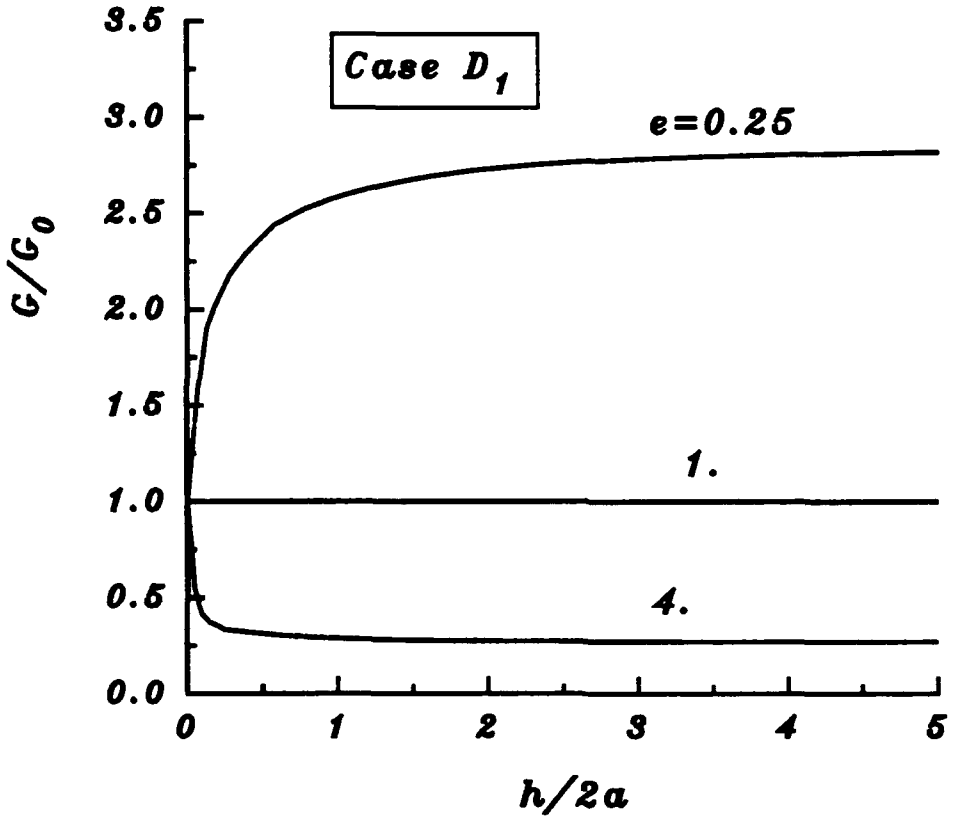


Fig. 12 Same as Fig. 7 material combination $D_1$, $e = E_{222}/E_3$, $G_{212} = E_{222}/2(1+\nu_3)$, medium 1 is high modulus carbon.

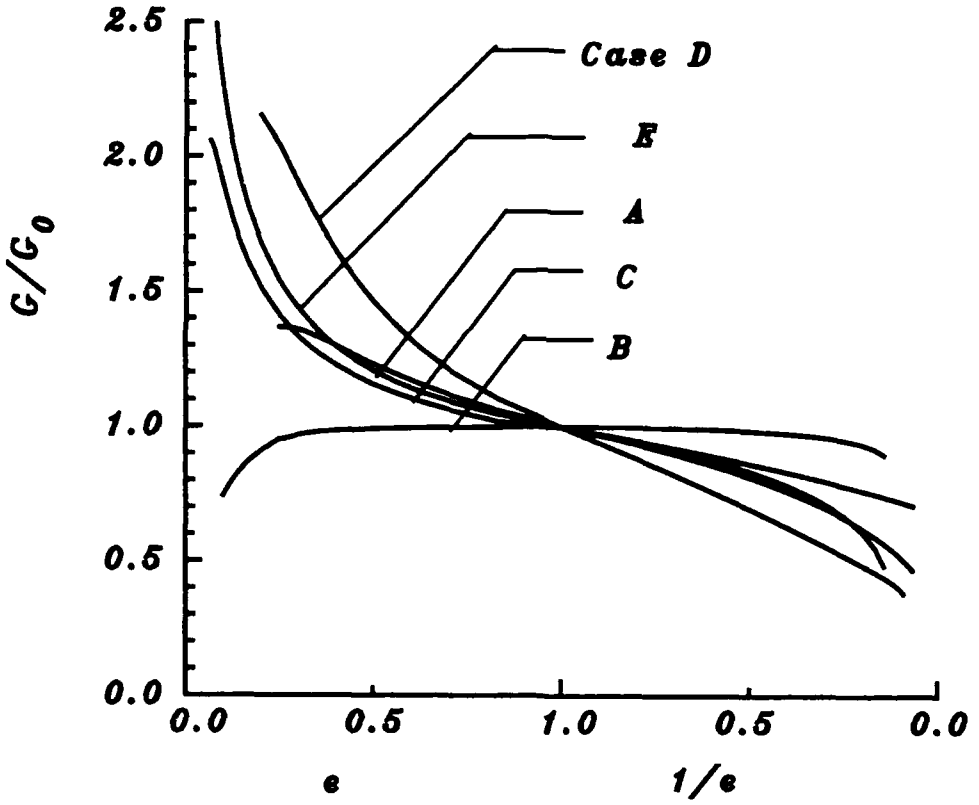


Fig. 13 Dependence of $\mathcal{G}$ on the variable $e$ for a single interface crack in bonded materials described in Table 3. h/2a = 0.4; $e = E_{211}/E_3$ in B and C, $e = E_{222}/E_3$ in A, D and $e = G_{212}/G_3$ in E.

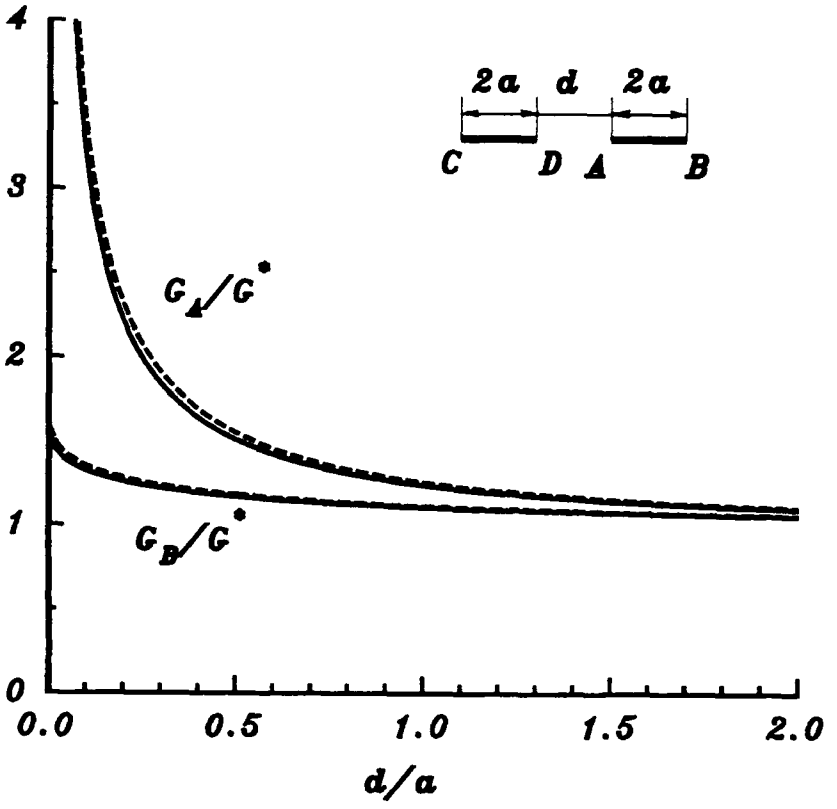


Fig. 14 Strain energy release rates for two equal collinear uniformly pressurized cracks in a homogeneous isotropic medium (full lines) and in two bonded dissimilar isotropic half spaces (dashed lines $E_2/E_1 = 15$, $\nu_1 = \nu_2 = 0.1$, $\omega = -0.1306$). In each case $\mathcal{G}^*$ is the corresponding single crack value (obtained from $d/a = \infty$), $\mathcal{G}_A/\mathcal{G}^* \to \infty$, $\mathcal{G}_B/\mathcal{G}^* \to 2$ for $d/a \to 0$ and $\mathcal{G}_A/\mathcal{G}^* \to 1$, $\mathcal{G}_B/\mathcal{G}^* \to 1$ for $d/a \to \infty$.

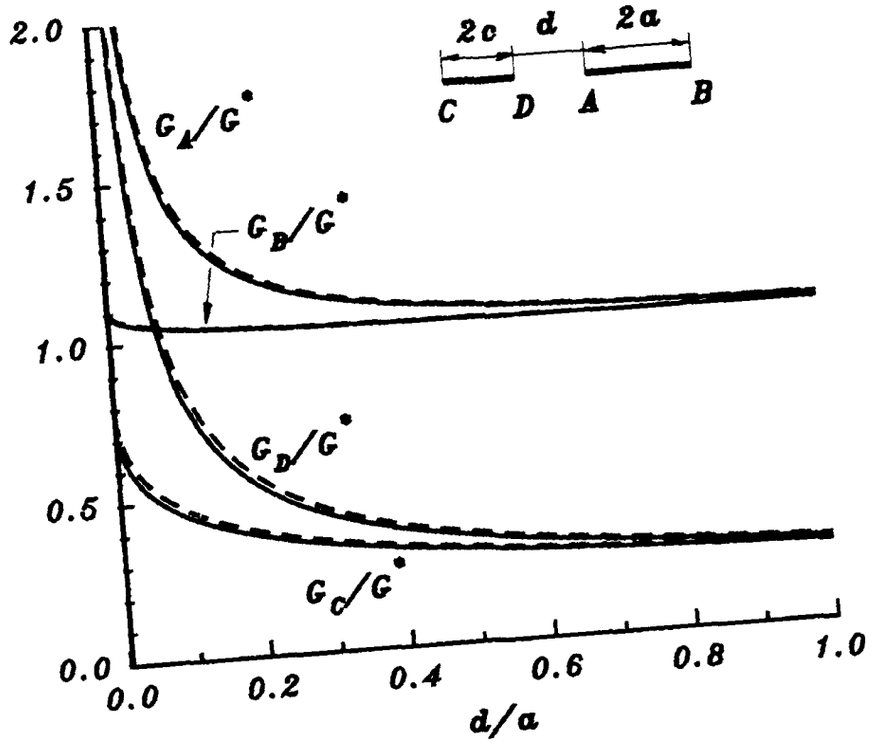


Fig. 15 Same materials as in Fig. 14 for two collinear cracks of lengths 2a and 2c. c/a = 0.2.

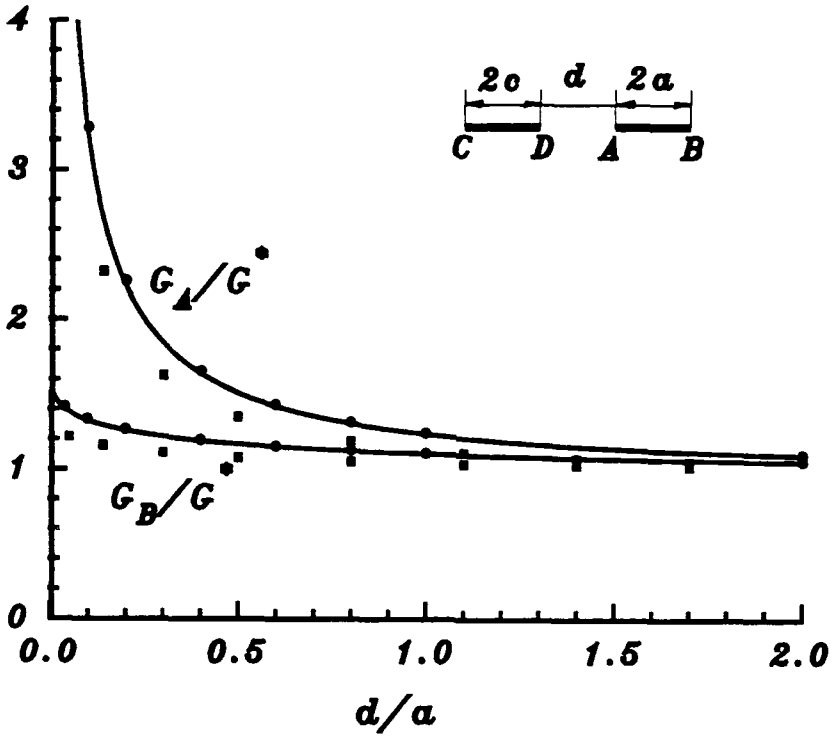


Fig. 16 Strain energy release rates for two collinear cracks of equal length (c = a) in an isotropic homogeneous plane (full lines, $\mathcal{G}^* = (1+\kappa)\sigma_0 a/S\mu$), in two bonded half planes (materials a and d, round dots, $h/2a = \infty$, $\mathcal{G}^* = 0.453\sigma_0{}^2 a$ $(GPA)^{-1}$) and in two half planes (materials a and c) bonded through a layer (material d) (square dots, $h/2a = 1$, $\mathcal{G}^* = 0.411\sigma_0{}^2 a$ $(GPA)^{-1}$), external load is uniform tension $\sigma_{22} = \sigma_0$ at infinity.

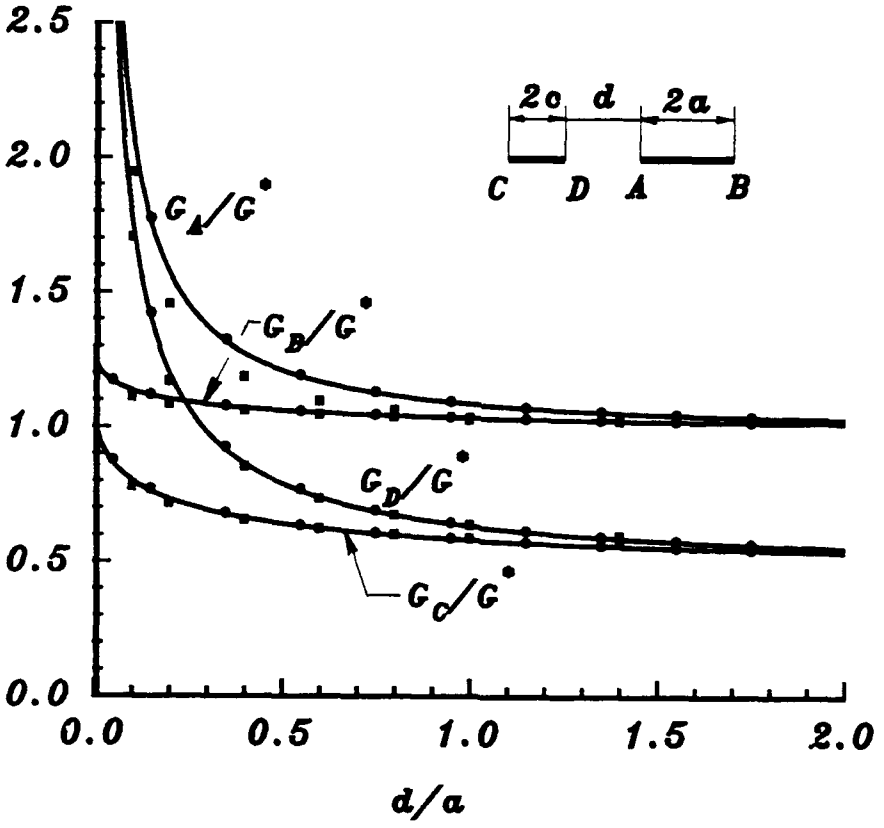


Fig. 17 Same materials and geometry as in Fig. 16, c/a = 0.5, D and A are the inner and C and B are the outer crack tips.

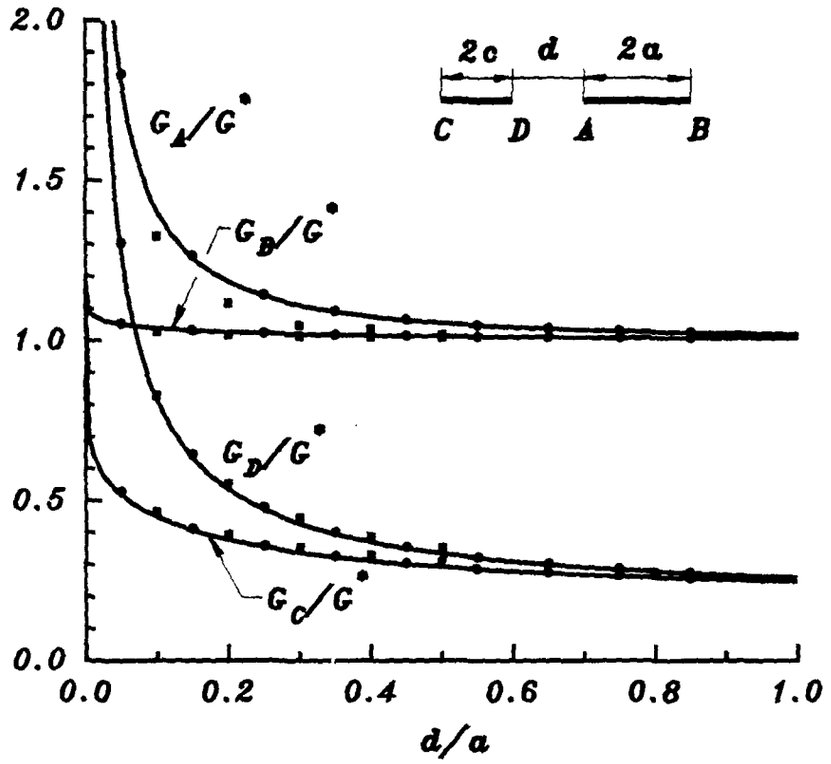


Fig. 18 Same as Fig. 16, c/a = 0.2.

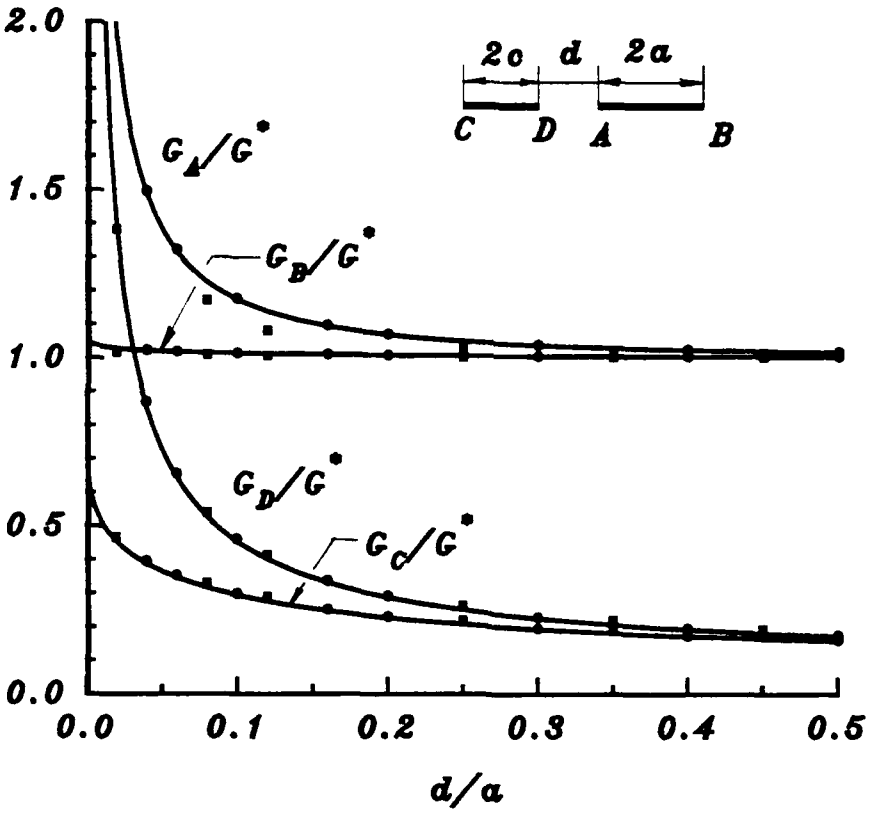


Fig. 19 Same as Fig. 16, c/a = 0.1.

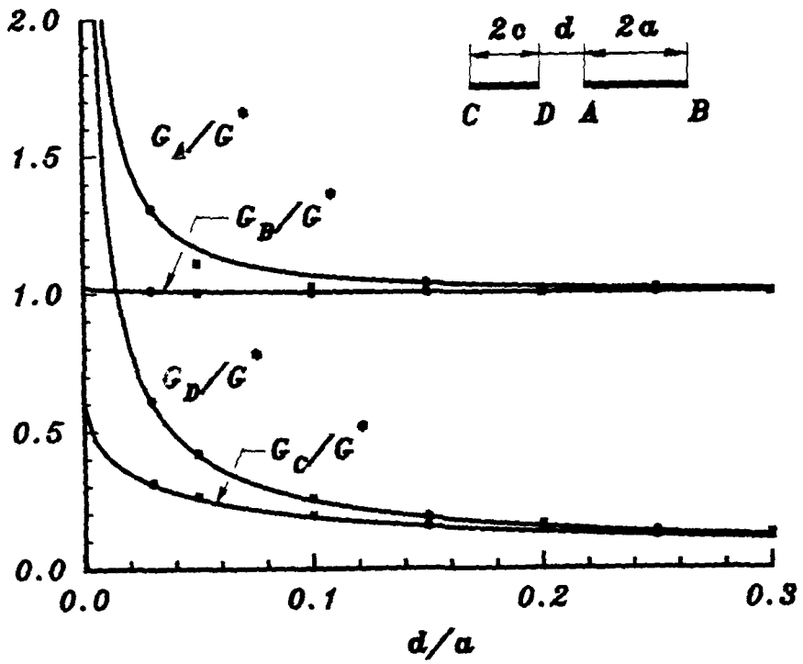


Fig. 20 Same as Fig. 16, c/a = 0.05.